EEFIT Research Grant Project

Rapid Earthquake Assessment Under Uncertain Conditions

Authors: Furkan Narlitepe & Vitor Silva

June/2025

Table of Contents

Page

1. Executive Summary

Rapid earthquake impact assessment systems are critical for guiding emergency response, yet they face inherent limitations during the first hours following major seismic events. This research investigates how rupture modeling approaches corresponding to the different levels of knowledge and uncertainty for the rupture geometry affect the accuracy of post-earthquake rapid impact estimates. The rupture modeling approaches adopted in the impact assessments are as follows:

- Point-source approximation (rupture as a single point)
- Planar rupture model (using nodal plane mechanisms)
- Pre-calculated rupture (from GEM Foundation's global hazard and fault models)
- Complex rupture models (published finite-fault solutions)

This study evaluates four modeling approaches across five well-known earthquakes with various magnitudes that occurred in different tectonic regimes around the world (Chile, Türkiye, Japan, Italy, and Spain). A set of scenario-based impact analyses was performed using the OpenQuake Engine, an open-source platform developed by the Global Earthquake Model (GEM) initiative, integrating hazard, global exposure, and vulnerability models. At the end, this study revealed significant variations in accuracy across rupture modeling approaches, with the point-source approximation showing particularly substantial differences - underestimating completely damaged buildings by up to 72% at the aggregated level for the Kahramanmaraş, Türkiye earthquake and reaching ~100% difference rates for the Iquique, Chile earthquake example, with even higher discrepancies at provincial scales. While the planar rupture model demonstrated improved accuracy compared to those obtained by the point-source approximation, the disparity across all regions remained significant, reflecting inherent modeling biases despite its advantage of incorporating focal mechanism data. The pre-calculated rupture model offered reliability with reasonable estimates, especially on the estimates across all regions/provinces, outperforming point-source approximations while remaining more practical than finite-fault solutions that need relatively more time to constrain rupture geometry. Crucially, analysis scale dramatically affected results, with regional assessments revealing differences typically double those at aggregated levels, particularly for high-magnitude events, highlighting the necessity of scale-sensitive interpretation in rapid impact assessments. This work provides actionable insights for national agencies and seismological institutions developing next-generation rapid earthquake assessment tools. By investigating an alternative rupture model for improving impact estimates during the critical first hours of an event, the research contributes to producing more effective rapid impact assessments following destructive earthquakes.

2. Introduction

Rapid impact assessments through real-time automated and/or non-automated systems are fundamental tools to assess the expected impact of destructive events and trigger the necessary measures to support the affected population. These assessments are also useful to identify regions where reconnaissance missions (such as those supported by EEFIT) to document earthquake damage should be deployed. However, such destructive events inherently involve “blind hours”, making rapid impact assessment impossible with precise clarity. On the other hand, it should be noted that the reports from past destructive events indicate that 85–95% of the successful rescues of people trapped under debris occurred within the first 24–48 hours (Huang et al., 2011). In this process, estimates are based on assumptions and approaches that are gradually refined as more data become available in the aftermath of an event. As an example of such approximations, seismic ruptures are often simplified as point sources, but this can introduce significant bias due to errors in the source-to-site distance estimation. For example, Monelli et al. (2014) found discrepancies up to 58% in design ground motion corresponding to the 475-year return period, while Lozano et al. (2024) noted a 65% PGA variation in the 2014 Napa earthquake due to limited data from the seismic stations and “Did you feel it?” (DYFI) responses. To improve accuracy, researchers have developed methods to refine distance metrics and incorporate finite-fault effects. Bommer and Akkar (2012) suggested separate regression parameters for point-source and rupture-based distances, though adoption has been limited. Hybrid models (e.g., Chiou and Youngs, 2014) unify these metrics, while others apply conversion factors (e.g., Thompson and Worden, 2018; Scherbaum et al., 2004; Kaklamanos et al., 2011; Worden and Wald, 2016) to adjust point-source distances, albeit with added uncertainty. Despite these efforts, inherent biases depending on approximated rupture distance remain, particularly for high-magnitude events, leading to uncertain impact assessments that require systematic quantification and mitigation.

The rapid assessment of earthquake impact requires three main components: an exposure model characterizing the built environment, a suite of damage functions, and the spatial distribution of ground shaking in the affected region. While all three components are affected by large epistemic and aleatory uncertainties, the estimation of the ground shaking is particularly challenging in the hours after the occurrence of strong events, especially in the Global South, where seismic networks are relatively sparse. In this context, three main sources of uncertainty can be identified: 1) the magnitude of the event, 2) the location of the epicenter, and most importantly, 3) the geometry of the seismic rupture. For the latter source of uncertainty, finite-fault solutions based on seismic and geodetic observations are arguably the most accurate method to constrain the seismic rupture, but are typically produced days or weeks after the event. A first-hand solution is to model the seismic rupture as a point-source, though such an approach is likely to

introduce large bias, particularly for large-magnitude events, due to discrepancies in the estimation of the source-to-site distances. It is thus clear that some gaps and limitations still exist in the field of rapid loss assessment, rendering impact estimates unreliable and potentially misleading.

This project aims to investigate discrepancies directly associated with rupture geometry uncertainty and its potential effect on the rapid impact estimates. For this purpose, we propose to explore different strategies to model rupture geometry, spanning from a simple point source to the creation of planar fault ruptures based on limited seismogenic information or the incorporation of pre-calculated ruptures using probabilistic seismic hazard models. We tested these different modeling options considering five well-known earthquake examples from Chile, Türkiye, Japan, Italy and Spain. To this end, we assess the performance of these approximated approaches on various loss metrics such as economic losses, fatalities and collapsed buildings, against complex rupture geometries published in the literature for these five events. Such analysis allow an understanding of what the expected discrepancies are for events of different magnitudes and which recommendations can be inferred to improve the accuracy and reliability of rapid impact estimates.

3. Statement of impact of research

Many automatic systems that produce reports for the evaluation of the post-earthquake impact have proven their usefulness after devastating earthquakes by providing valuable information to governments, emergency responders, damage surveyers, and the private sector. However, highly destructive earthquakes inevitably involve “blind hours” during which the impact cannot be effectively assessed. In such blind hours, predictions proceed through a series of approximations, simplifications, and corrections. For instance, the USGS PAGER system (Earle et al., 2009; Wald et al., 2020), undoubtedly the most well-known and mature platform for rapid impact assessment in the world, provides several updates of their impact metrics in the hours and days after destructive events (see Figure 1). Our proposed method to combine limited information generally available minutes after the occurrence of seismic events (i.e., magnitude, location, depth, moment tensor) with pre-calculated seismic ruptures from the global mosaic of source models of the Global Earthquake Model (GEM) Foundation has the potential to significantly reduce the discrepancies in impact assessment, even within minutes of the event. We believe that the outcomes from this research can be useful to national authorities and international organizations with the remit to calculate and communicate earthquake impact shortly after their occurrence, in particular when there is an urgent need to deploy rescue teams and other human resources for disaster relief.

Such results are also useful for the scientific community, which is often responsible for developing and operating rapid loss assessment platforms.

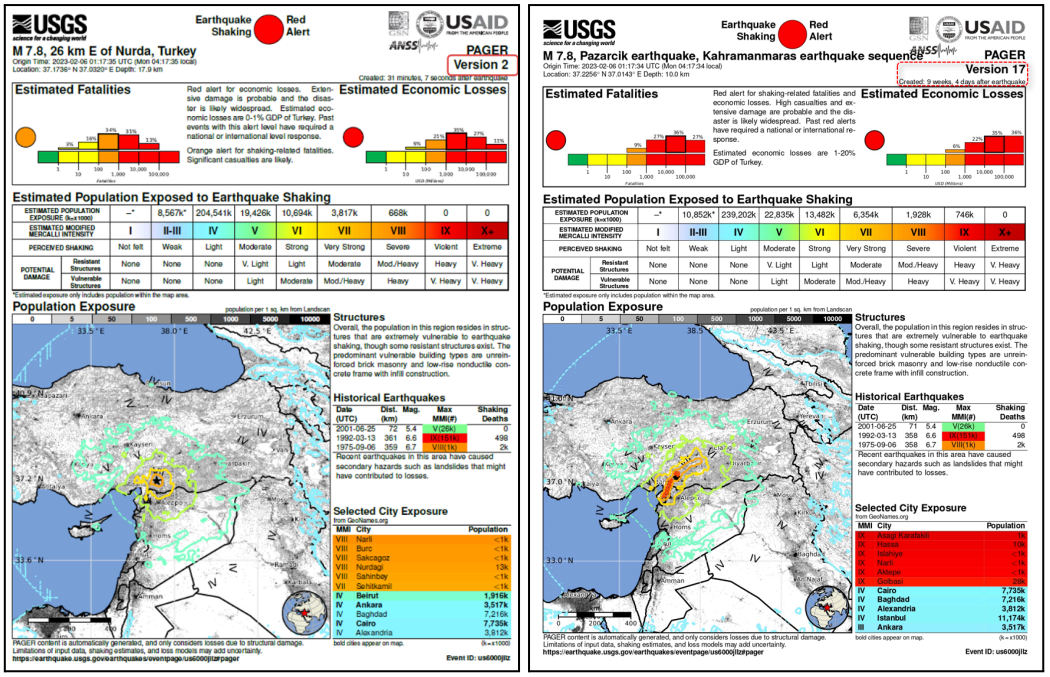

Figure 1. OnePAGER (2nd and 17th versions) released by the USGS's PAGER system for the M7.8 Kahramanmaraş earthquake sequence.

4. Input models for performing risk assessments

a. Selection of Earthquake Examples

To comprehensively evaluate the influence of rupture modeling approaches on earthquake impact assessments, this study leverages five real-world examples from geographically diverse tectonic regimes. These events were intentionally selected based on the following criteria:

1) **Magnitude Diversity:** A broad range of magnitudes (from M5.1 to M8.2) to assess the influence of rupture size.
2) **Location Variability:** An inland rupture beneath an urbanized area (2007 M7.0 Kumamoto, Japan). An offshore event within 30 km of urban centers (2014 M8.2 Iquique, Chile).
3) **Geometric Complexity:** A rupture with an arcuate shape, challenging to represent with a simple planar geometry (2023 M7.8 Kahramanmaras, Türkiye).
4) **Built Environment Contrast:** Regions with varying construction practices, from vulnerable housing (e.g., Italy, Türkiye) to code-compliant structures (e.g., Japan).

b. Exposure, Site and Vulnerability Models

For each scenario, the global exposure model developed by Estrada-Yepes et al. (2023) is employed. The exposure models for each region are publicly available in the GitHub repository featured in the associated publication, and they cover residential, commercial, and industrial buildings. Additionally, a region-specific site model is utilized for each scenario to conduct a comprehensive risk analysis. The fragility and vulnerability functions (see Martins and Silva, 2020) cover all building classes within the exposure model. Using the OpenQuake Engine (Pagani et al. 2014; Silva et al. 2014), an open-source software for hazard and risk calculations developed by the GEM initiative, ground shaking and risk estimates were generated considering various loss metrics for each combination of earthquake scenario and rupture modeling approach. These loss metrics encompass economic losses, fatalities, and the number of completely damaged buildings. The impact assessments are conducted for each simplified rupture modeling approach, as well as considering the benchmark complex rupture gathered from the literature. The differences (Δ) are analyzed for the total number of damaged buildings ($\Delta_{i=all}$), as well as for the number of buildings disaggregated at the first administrative division (Δ_i) for a more granular understanding, as expressed by Eq. 1:

$$\Delta_i = \left| N|DS4_{E,i} - N|DS4_{R,i} \right| \quad (1)$$

Where $N|DS4_{E,i}$ and $N|DS4_{R,i}$ represents the estimated and reference number of buildings with complete damage (DS4) for administrative division i, or for the entire region (i.e., all divisions). These values are also presented as a percentage ($\Delta_{\%,i}$), by normalizing the differences by $N|DS4_{R,i}$. Finally, the weighted absolute percent differences across all administrative divisions are calculated, as expressed by Eq. 2:

$$Weighted\ absolute\ \Delta_{\%} = \sum_{n=j}^{i} \left| \frac{\Delta_{\%,i} \times N|DS4_{R,i}}{N|DS4_{R,i=all}} \right| \quad (2)$$

Where j is the number of administrative divisions with buildings with complete damage. This is an important metric that allows evaluating the performance of the modeling approaches across all regions, which might not be visible in the total impact due to the averaging effect, as further discussed in Section 6. Regarding the ground motion characterization, Table 1 presents the employed ground motion models (GMMs) and their corresponding weight factors. These are incorporated into a logic tree framework to account for epistemic uncertainty associated with the selection of ground motion models. It is important to note that, to optimize clarity and conciseness, the spatial distribution of ground shaking estimates (i.e., peak ground acceleration (PGA)) will be presented for a single representative GMM in subsequent sections. Additionally, the

economic losses are limited to direct losses encompassing structural damage, non-structural damage, and building contents. Indirect losses, such as business interruption and loss of human capital, are not included in the current scope.

c. Rupture Models

This section provides a description of the individual rupture modeling approaches employed in this study, emphasizing how these methods constrain rupture geometry. Four distinct rupture modeling approaches, characterized by varying levels of uncertainty, are considered:

1. **Point-Source Approximation:** This approach, commonly utilized in initial rapid impact assessments, relies heavily on limited information and exhibits significant uncertainties. Due to the scarcity of data immediately following an earthquake, the calculation is primarily based on the earthquake's magnitude and location. This simplification leads to an unconstrained rupture geometry, resulting in substantial biases in ground motion estimates. Specifically, the distance between the asset and the epicenter (R_{EP}) is directly used in ground motion models, rather than other more accurate rupture-to-site distances (e.g., R_{rup}, R_{JB}). This approximation inevitably leads to an underestimation of the ground shaking, particularly for large-magnitude events.
2. **Planar Rupture Model:** This approach incorporates focal mechanism solutions obtained from international seismic networks (e.g., AFAD and USGS) and national agencies within a few minutes of the event. By incorporating information on strike, dip and rake angles, the planar rupture model provides a more constrained representation of the rupture geometry compared to the point-source approximation.
3. **Pre-Calculated Rupture Model:** This approach utilizes pre-computed rupture models derived from probabilistic seismic hazard assessment (PSHA) models. This method uses a rupture matching algorithm based on the hypocenter location, magnitude and focal mechanism, to select a rupture from the seismic sources in the GEM Mosaic of Hazard Models.
4. **Complex Rupture Model:** This approach, considered the most sophisticated and accurate, leverages finite fault solutions derived from seismic waveform data, GPS measurements, and other geophysical observations. These data are used to determine the earthquake's characteristics (magnitude, depth, location, and faulting type) and subsequently model the spatial and temporal distribution of slip on the fault plane through techniques such as kinematic and dynamic inversion. Albeit providing the most realistic representation of the rupture process, the development of a finite fault solution can be a time-consuming

process, often requiring weeks or even months, particularly for large-magnitude earthquakes.

Table 1 summarizes the nodal plane solutions used to constrain the rupture geometry in the planar rupture models and provides details on the finite fault solutions obtained from the SRCMOD database (Mai et al., 2014), which is a publicly available repository of finite fault models used to develop the complex rupture models, along with general information for the earthquake scenarios employed in this study.

Table 1. Nodal plane and finite-fault solutions utilized for the planar and the complex rupture models, along with the GMMs weight factors adopted for ground motion characterization.

Earthquake Scenario	M_w	Depth	Faulting Mechanism	Nodal Plane Solution			Finite-Fault Solution	GMM	Weight Factor
(Country)	(USGS)	(km)		Strike	Dip	Rake			
Iquique (Chile)	8.2	25.0	Thrust	[a]358°	12°	107°	Hayes et al. (2010)	Abrahamson et al. (2015) Montalva et al. (2017) Zhao et al. (2006)	0.33 0.33 0.34
Kahramanmaras (Türkiye)	7.8	8.6	Strike-slip	[b]233°	74°	18°	[c]	Akkar et al. (2014) Cauzzi et al. (2014) Zhao et al. (2006)	0.33 0.33 0.34
Kumamoto (Japan)	7.0	10.0	Strike-slip	[d]224°	66°	-152°	Yagi et al. (2016)	Chiou and Youngs (2014) Boore et al. (2014) Zhao et al. (2016)	0.35 0.35 0.30
L'Aquila (Italy)	6.3	8.8	Normal	[e]121°	43°	-124°	Gallovič et al. (2015)	Bindi et al. (2014) Cauzzi et al. (2014) Kotha et al. (2020)	0.33 0.33 0.34
Lorca (Spain)	5.1	1.0	Strike-slip	[f]233°	45°	42°	Lopez-Camino et al. (2016)	Zhao et al. (2016) Cauzzi et al. (2014) Akkar et al. (2014)	0.35 0.35 0.30

[a]: https://earthquake.usgs.gov/earthquakes/eventpage/usc000nzvd/moment-tensor

[b]: https://deprem.afad.gov.tr/event-detail/408326

[c]: https://earthquake.usgs.gov/product/shakemap/us6000jllz/us/1675660631596/download/rupture.json

[d]: https://earthquake.usgs.gov/earthquakes/eventpage/us20005iis/moment-tensor

[e]: https://earthquake.usgs.gov/earthquakes/eventpage/usp000gvtu/moment-tensor

[f]: https://earthquake.usgs.gov/earthquakes/eventpage/usp000j1en/moment-tensor

5. Impact Assessment Results for Earthquake Examples

a. 2014 M8.2 Iquique, Chile Earthquake

On 1 April 2014, the Chile earthquake, with a magnitude of M_w = 8.2, struck the coastline of northern Chile, marking it as one of the most important seismic events in recent history. This earthquake occurred at a depth of 25 km and was generated by a thrust faulting mechanism within the boundary region of the Nazca and South American tectonic plates (Hayes et al., 2016). Official statistics from the National Institute for Civil Defense (INDECI) indicate that the event resulted in approximately 11 fatalities and 209 injuries. Furthermore, the earthquake caused varying degrees of damage to an estimated 8,300 houses. The Iquique earthquake with a magnitude of M_w = 8.2 was selected in this study as an earthquake example representing a strong earthquake located offshore to investigate the influence of the rupture modeling approaches on the various risk metrics, such as economic loss, the number of fatality estimates, and the number of completely damaged buildings. The ground shaking estimates (i.e., PGA) were performed considering the exposure and site models, along with the set of GMMs specified in the previous section.

i. PGA estimates for the Iquique earthquake example

For the sake of brevity, the PGA estimates corresponding to each rupture model are depicted for only the GMM developed by Montalva et al. (2017) in Figure 2. Based on the results provided in Figure 2, it is observed that the impact area and the value of PGA estimates are highly conditional on the geometry and orientation of the rupture. For instance, the point-source approximation led to an affected area with a quite narrow extent and relatively low PGA estimates varying from 0.16g to 0.19g on some parts of the coastline of the Arica Y Parinacota and Tarapaca regions. For the planar rupture, the affected area substantially expanded by covering almost the whole length of the coastline of both regions, and the PGA ranges between 0.29g and 0.36g. The pre-calculated rupture model gave a relatively similar spatial distribution for the PGA estimates compared to that of the planar rupture. However, the affected area shifted to the inner part of cities and slightly higher PGAs with up to 0.40g were achieved, especially in the Tarapaca region. Finally, the complex rupture model produced a substantially similar affected area to the planar rupture model, with the only difference being that it yielded higher PGA estimates in the Tarapaca region, depending on its location along the coastline.

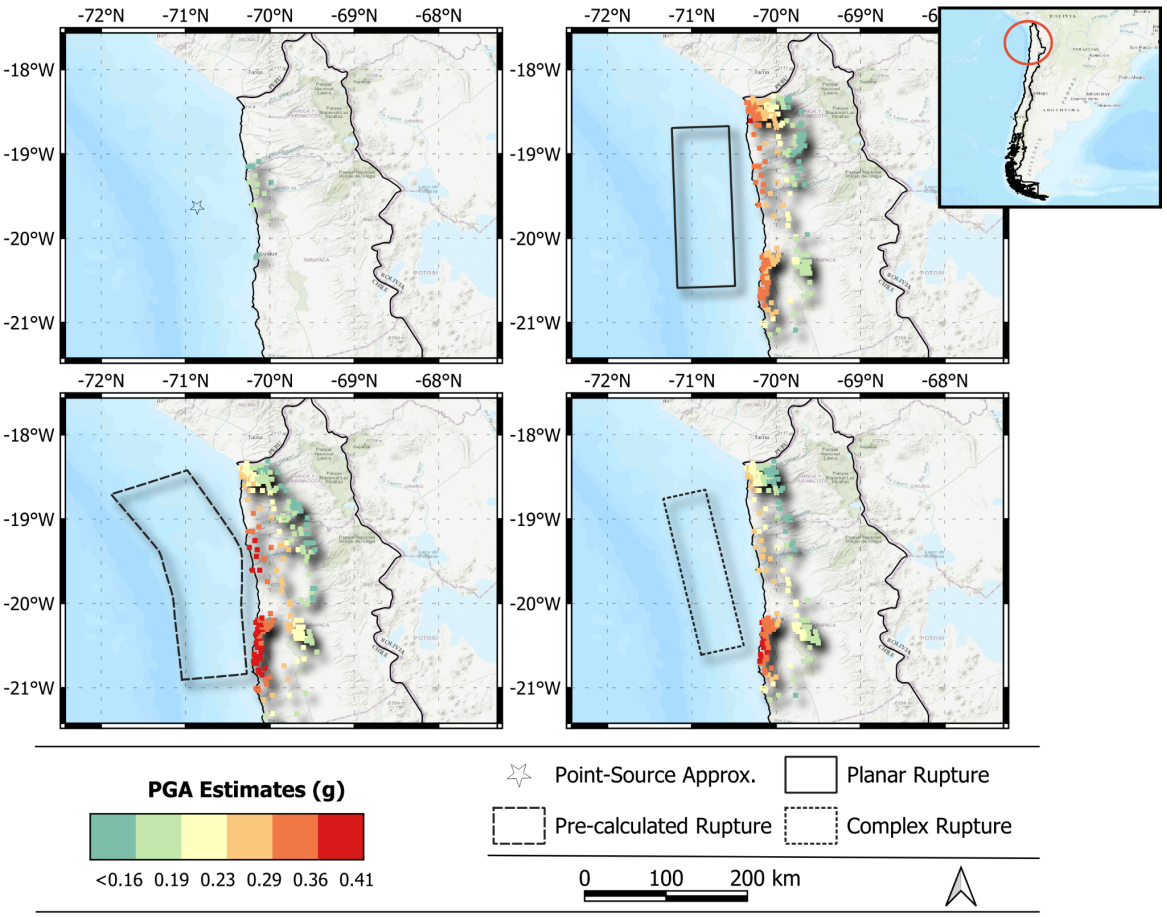

Figure 2. The spatial distribution of PGA estimates for each rupture modeling approach for the Iquique earthquake example.

ii. Economic loss estimates for the Iquique earthquake example

As for the loss assessment, the spatial distribution of the economic losses for the Iquique earthquake example is presented in Figure 3 for each rupture modeling approach. In general, the geographic distribution of the economic loss estimates significantly varied depending on the rupture modeling approaches, in line with the distribution pattern of the PGA. For example, the point-source approximation resulted in the lowest economic loss estimates, while the planar and pre-calculated rupture model led to an increase of economic losses ranging from \$1.0 to \$1.8 billion USD in the Arica Y Parinacota and Tarapaca regions. Similarly, the complex rupture model produced a broader distribution pattern covering both regions. The economic losses for each rupture model and their associated difference rates based on the complex rupture model are summarized in Table 2 at both the aggregate and regional levels. When the loss estimates are examined at the aggregated level rather than at the regional scale, the total economic losses obtained using the point-source approximation is around 20.2 million USD with a difference rate of almost 100%, while the planar and the pre-calculated rupture models resulted in 2.1 billion USD and 2.3 billion USD, with associated difference rates of 12% and 20%, respectively, compared

to those obtained using the complex rupture model. However, for the offshore earthquake example, the pre-calculated rupture model led to better economic loss estimates across all regions, with a discrepancy of approximately 20%.

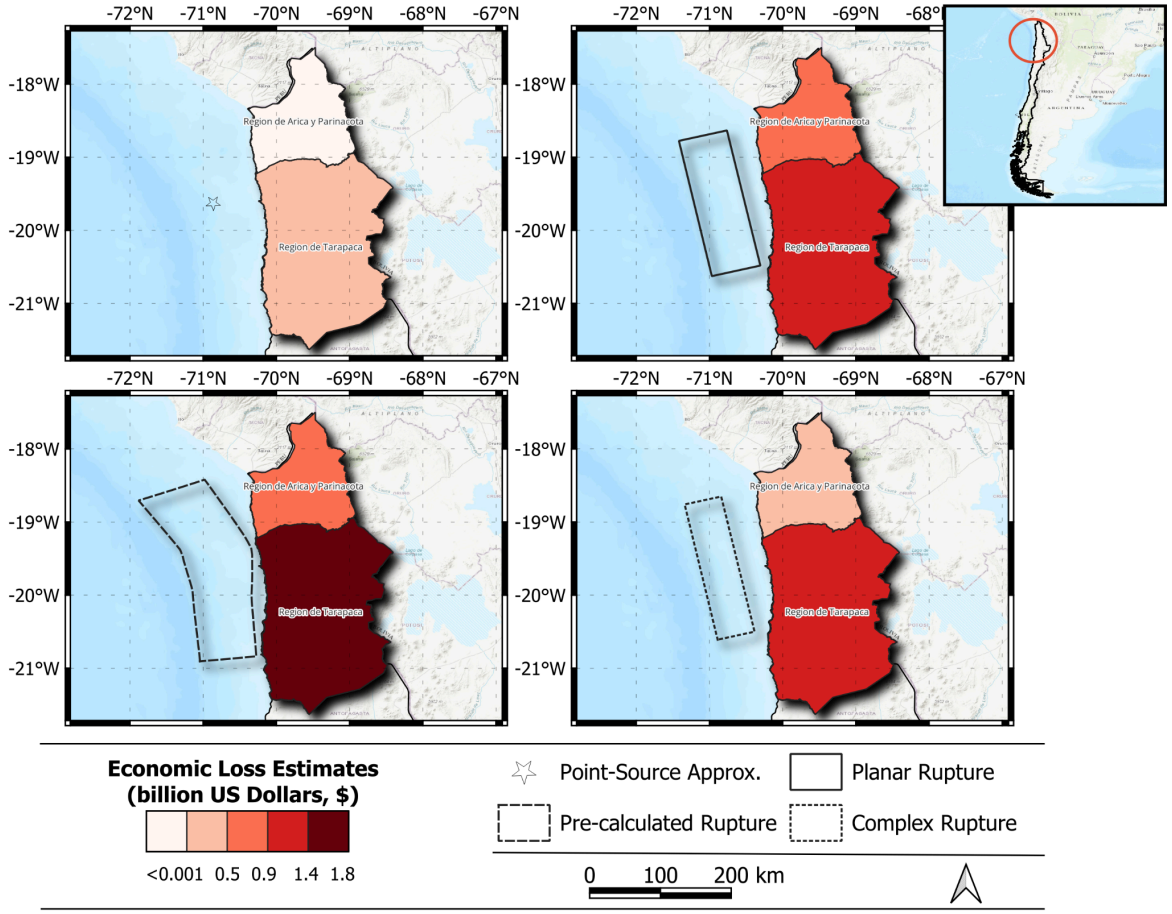

Figure 3. Spatial distribution of economic loss estimates for each rupture modeling approach for the Iquique earthquake example.

Table 2. Mean economic loss estimates disaggregated by region for each rupture modeling approach for the Iquique earthquake example.

Region	Economic Loss Estimates (Million US Dollars)			
	Point-Source	Planar	Pre-Calculated	Complex Finite
Region De Arica Y Parinacota	0.4 (100%)	872.1 (87%)	509.6 (10%)	465.4
Region De Tarapaca	19.8 (99%)	1,248.5 (12%)	1,761.5 (24%)	1,421.9
Total	**20.2 (99%)**	**2,120.5 (12%)**	**2,271.2 (20%)**	**1,887.3**
Weighted Regional Difference	**99%**	**31%**	**20%**	**-**

iii. Fatality estimates for the Iquique earthquake example

The number of fatality estimates and the associated difference rates are summarized in Table 3, with results presented at both the aggregate and regional levels for each rupture model. Upon examining the estimates at the aggregated level, the total estimated number of fatalities by point-source approximation is approximately 1 people with a difference rate of 99%, while the planar and pre-calculated rupture models resulted in similar estimates of 145 and 147, with difference rates of 17% and 18%, respectively. As for the comparison across all regions, the pre-calculated rupture model gave the best estimates with the lowest discrepancy, while the difference rate of the planar rupture model increased up to 36%.

Table 3. Mean number of fatality estimates disaggregated by region for each rupture modeling approach in the Iquique earthquake example.

Region	Number of Fatality Estimates (person)			
	Point-Source	Planar	Pre-Calculated	Complex Finite
Region De Arica Y Parinacota	-	67 (95%)	38 (10%)	34
Region De Tarapaca	1 (99%)	78 (13%)	109 (21%)	90
Total	**1 (99%)**	**145 (17%)**	**147 (18%)**	**125**
Weighted Regional Difference	**99%**	**36%**	**18%**	-

iv. Number of completely damaged buildings estimates for the Iquique earthquake example

Figure 4 illustrates the spatial distribution of completely damaged buildings for each rupture modeling approach, while Table 7 summarizes the aggregated and regional results. As shown in the table, the mean total number of completely damaged buildings is approximately 55 when using the point-source approximation, which also exhibits the highest discrepancy—up to 99%. In contrast, the planar and pre-calculated rupture models estimate 6,974 and 7,280 completely damaged buildings, with relative differences of 14% and 19%, respectively. When evaluating impacts across all regions, the pre-calculated rupture model provides the most consistent estimates, showing the lowest discrepancy in total building damage (19%). In comparison, the planar rupture model shows greater regional variation, with differences reaching up to 35%.

Table 4. Mean number of completely damaged buildings estimates disaggregated by region for each rupture modeling approach in the Iquique earthquake example.

Region	Number of Completely Damaged Buildings Estimates			
	Point-Source	Planar	Pre-Calculated	Complex Finite
Region De Arica Y Parinacota	2 (100%)	2,994 (103%)	1,626 (10%)	1,476
Region De Tarapaca	53 (99%)	3,979 (14%)	5,654 (22%)	4,624
Total	**54 (99%)**	**6,974 (14%)**	**7,280 (19%)**	**6,100**
Weighted Regional Difference	**99%**	**35%**	**19%**	-

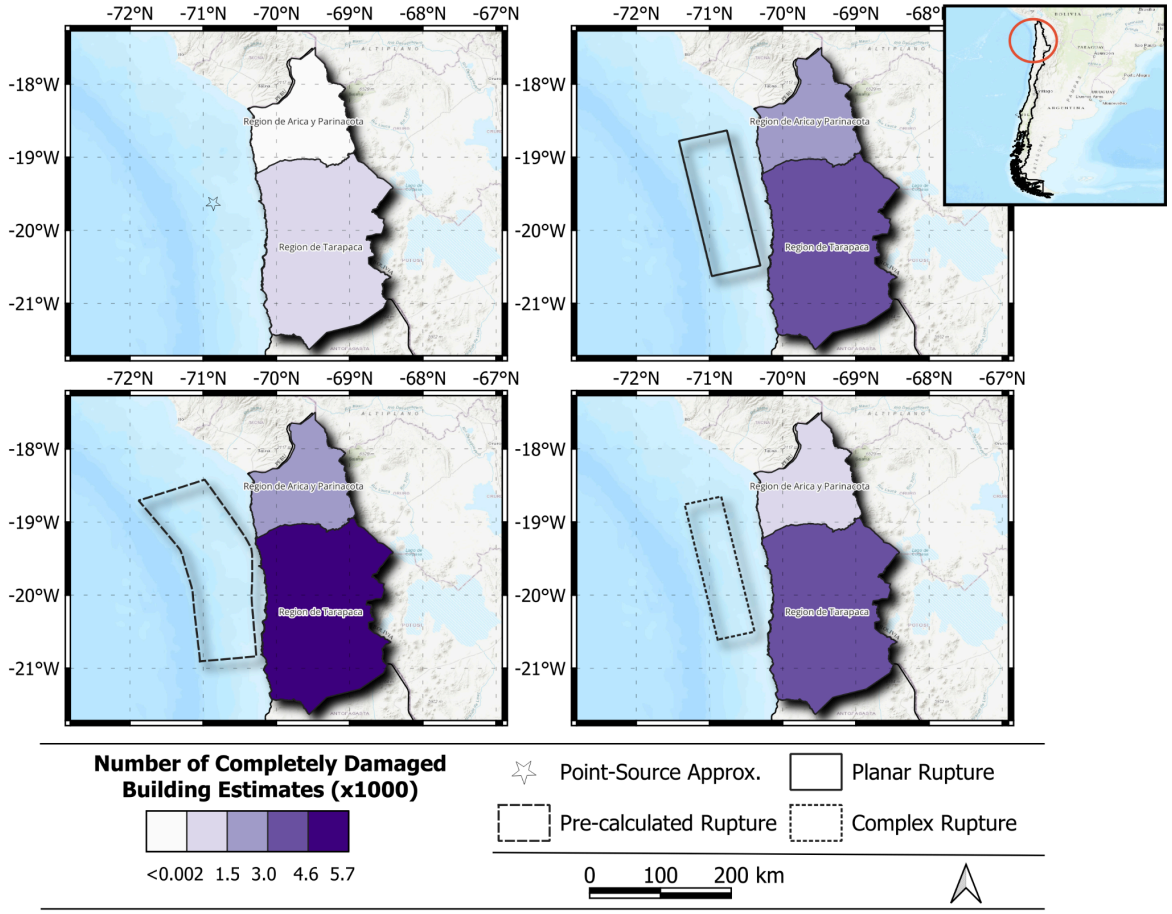

Figure 4. The spatial distribution of the number of completely damaged buildings estimates obtained by each rupture modeling approach for the Iquique earthquake example.

b. 2023 M7.8 Kahramanmaraş, Türkiye Earthquake

On 6 February 2023, the Kahramanmaras earthquake sequence, comprising two major events with magnitudes of M_w = 7.8 and 7.5, struck southern Türkiye and northern Syria. These earthquakes resulted from strike-slip faulting along the active North Anatolian Fault Zone (NAFZ), with hypocentral depths of 8.6 km and 7.0 km, respectively. According to the latest AFAD reports, the destructive sequence affected 11 provinces, causing catastrophic destruction: nearly 50,000 fatalities, 115,000 injuries, and the collapse of 38,000 buildings. Additionally, over 90,000 reinforced concrete (RC) structures sustained severe damage (AFAD, 2023; Narlitepe et al., 2024). This study focuses on the first M_w = 7.8 due to its distinctive arcuate rupture geometry. The ground shaking estimates (i.e., PGA) were performed considering the exposure and site models, along with the set of GMMs specified in the previous section.

i. PGA estimates for the Kahramanmaras earthquake example

For the sake of brevity, Figure 5 presents the PGA estimates for each rupture model using exclusively the GMM developed by Akkar and Cagnan (2014). The results clearly demonstrate that the spatial distribution of PGA values is highly correlated with the rupture geometry prescribed by each modeling approach. The point-source approximation, while computationally simple, generated localized PGA estimates of 0.22g to 0.40g confined to the immediate epicentral area. In contrast, the planar rupture model produced both higher PGA values and a more extensive spatial distribution of ground shaking. Most significantly, the pre-calculated rupture model yielded the most comprehensive shaking pattern among the other approximated rupture models. This model not only predicted the widest affected area but also showed excellent agreement with the actual complex rupture characteristics of the event, generating PGA values between 0.5g and 0.8g, particularly in near-fault regions.

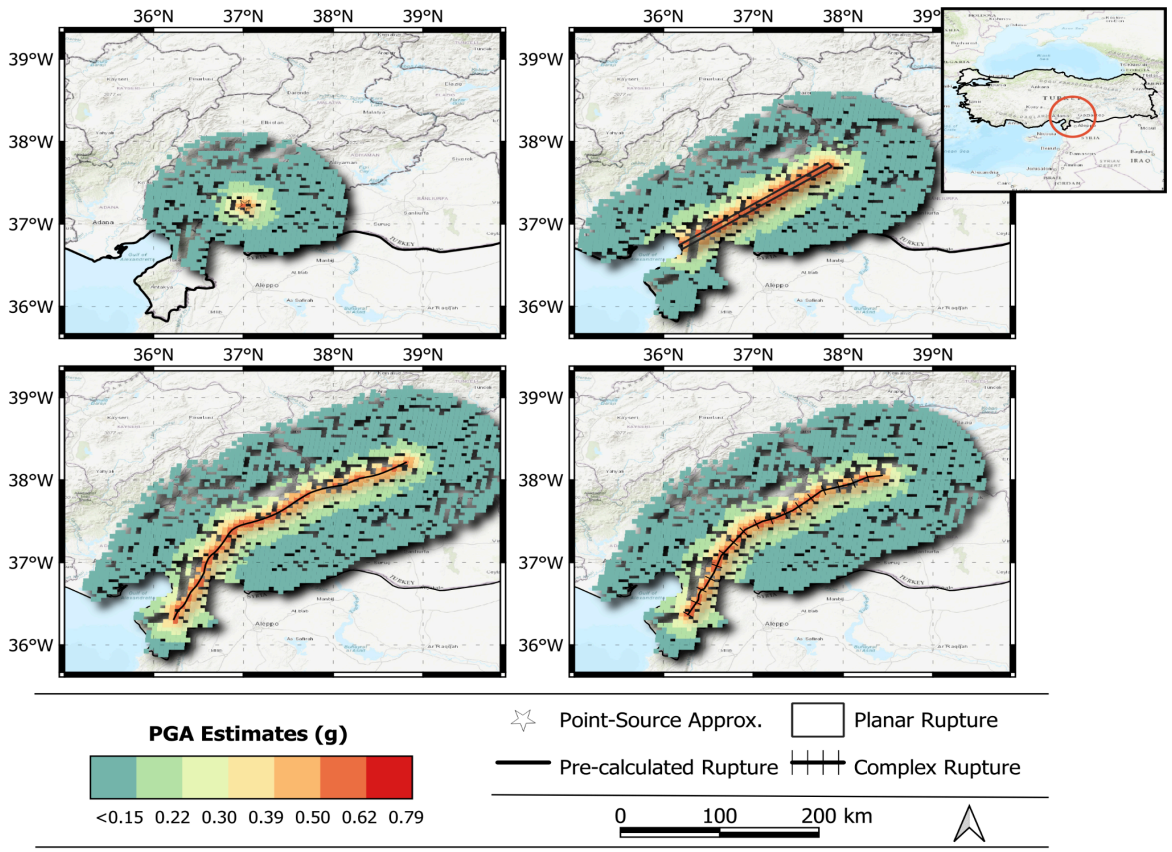

Figure 5. The spatial distribution of PGA estimates for each rupture modeling approach for the Kahramanmaras earthquake example.

ii. Economic loss estimates for the Kahramanmaras earthquake example

The economic assessment results for the Kahramanmaras earthquake scenario are presented in Figure 6, showing the spatial distribution of estimated economic losses across different rupture modeling approaches. The loss patterns exhibit strong correlation with the corresponding PGA distributions. The point-source approximation, while computationally simple, produced the most conservative estimates, both in terms of affected area and total losses. This approach predicted economic losses primarily concentrated near the epicenter, with Gaziantep province showing estimated damages ranging from 2.9 to 6.1 million USD. The limited spatial extent of these estimates reflects the model's inherent simplification of rupture geometry. In contrast, more sophisticated models incorporating detailed fault geometry and orientation parameters revealed significantly different loss patterns. The planar, pre-calculated, and complex rupture models all predicted both higher total losses and broader spatial impacts. These approaches extended the 2.9–6.1 million USD loss range to include two additional provinces (Kahramanmaras and Hatay).

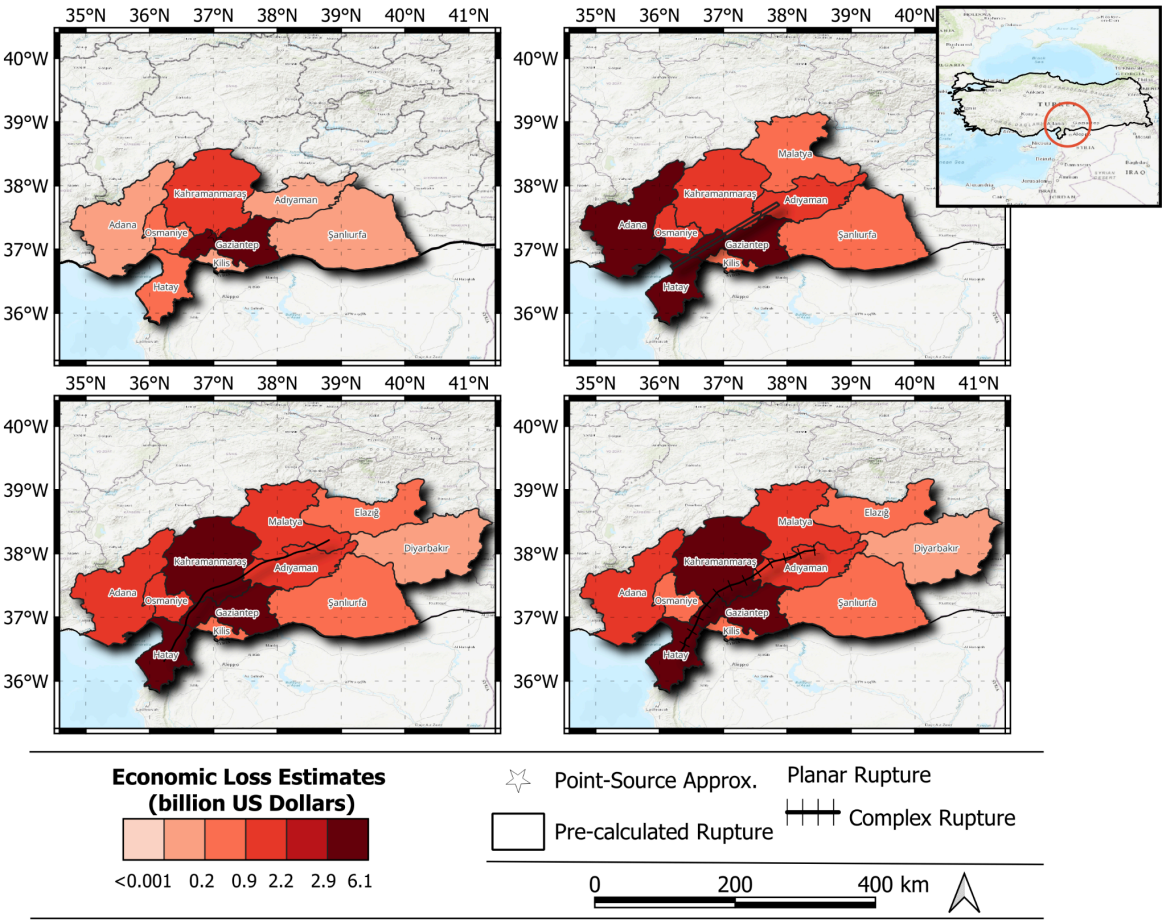

Figure 6. Spatial distribution of economic loss estimates for each rupture modeling approach in the Kahramanmaraş earthquake example.

Table 5 summarizes the economic loss estimates and their corresponding difference rates for each rupture model, presenting both aggregate and province-level results. At the aggregate level, the point-source approximation yields a total economic loss estimate of approximately 7.3 billion USD, showing a 61% difference compared to that of the complex rupture model. In contrast, the planar and pre-calculated rupture models produce substantially higher estimates of $20.2 billion and 19.1 billion USD, with significantly lower difference rates of 2% and 7%, respectively. However, aggregate-level analysis alone proves inadequate and potentially misleading, as demonstrated in our previous Iquique earthquake case study. When examining provincial-level results, the performance ranking of models changes notably. The pre-calculated rupture model emerges as the most accurate approach across all regions, exhibiting the lowest overall discrepancy (15%) when compared to approximated rupture models. Meanwhile, the planar rupture model's difference rate increases dramatically from 2% at the aggregate level to 51% at the provincial level.

Table 5. Mean economic loss estimates disaggregated by province for each rupture modeling approach in the Kahramanmaras earthquake example.

Province	Economic Loss Estimates (Million US Dollars)			
	Point-Source	Planar	Pre-Calculated	Complex Finite
ADANA	16.8 (99%)	3,603.1 (195%)	952.3 (22%)	1,220.7
ADIYAMAN	64.7 (96%)	1,139.5 (22%)	1,520.7 (4%)	1,457.3
DİYARBAKIR	-	-	108.7 (461%)	19.4
ELAZIĞ	-	-	782.8 (165%)	295.0
GAZİANTEP	4,781.8 (28%)	6,070.3 (62%)	3,590.9 (4%)	3,742.9
HATAY	229.8 (95%)	4,176.4 (14%)	5,882.3 (21%)	4,855.4
MALATYA	0.2 (100%)	676.4 (65%)	1,909.4 (0%)	1,907.5
K.MARAŞ	1,529.9 (62%)	1,992.1 (51%)	3,738.4 (8%)	4,050.2
ŞANLIURFA	43.5 (85%)	304.7 (8%)	348.5 (23%)	282.5
KİLİS	149.8 (10%)	195.1 (17%)	164.3 (1%)	166.5
OSMANİYE	472.3 (43%)	1,070.8 (30%)	1,087.1 (32%)	822.5
Total	**7,288.8 (61%)**	**19,228.4 (2%)**	**20,085.4 (7%)**	**18,819.8**
Weighted Regional Diff.	**72%**	**51%**	**15%**	-

iii. Fatality estimates for the Kahramanmaras earthquake example

Table 6 presents fatality estimates and corresponding difference rates for each rupture model, comparing aggregate and province-level results. At the national level, the point-source approximation substantially underestimates fatalities (3,515; 65% difference rate), while the planar (9,809; 2%) and pre-calculated (10,737; 7%) rupture models show markedly improved accuracy. However, provincial-level analysis demonstrates even greater model performance disparities, particularly in the most affected provinces (Kahramanmaras, Hatay, and Gaziantep). In the Kahramanmaras province, the point-source approximation shows poor accuracy (68% difference rate), while the planar (55%) and pre-calculated (11%) models demonstrate progressively better performance. Across all provinces, the pre-calculated rupture model achieves superior accuracy with the lowest overall discrepancy (16%), followed by the planar model. The complex rupture model serves as the reference for these comparisons.

Table 6. Mean number of fatality estimates disaggregated by province for each rupture modeling approach in the Kahramanmaras earthquake example.

Province	Number of Fatality Estimates (person)			
	Point-Source	Planar	Pre-Calculated	Complex Finite
ADANA	6 (99%)	1,392 (197%)	347 (26%)	469
ADIYAMAN	32 (97%)	770 (21%)	1,012 (4%)	971
DİYARBAKIR	-	-	81 (789%)	9
ELAZIĞ	-	-	292 (242%)	85
GAZİANTEP	2,402 (32%)	3,223 (77%)	1,727 (5%)	1,816
HATAY	101 (96%)	2,145 (21%)	3,290 (22%)	2,702
MALATYA	-	358 (71%)	1,247 (2%)	1,225
K.MARAŞ	609 (68%)	870 (55%)	1,712 (11%)	1,931
ŞANLIURFA	49 (81%)	338 (33%)	314 (23%)	254
KİLİS	83 (15%)	117 (21%)	94 (3%)	97
OSMANİYE	233 (47%)	596 (35%)	621 (41%)	440
Total	**3,516 (65%)**	**9,809 (2%)**	**10,737 (7%)**	**10,001**
Weighted Regional Difference	**77%**	**54%**	**16%**	**-**

iv. Number of completely damaged buildings estimates for the Kahramanmaras earthquake example

Figure 7 illustrates the spatial distribution of the estimated number of completely damaged buildings for each rupture modeling approach. Table 7 further quantifies these estimates, presenting both aggregate and province-level results along with their corresponding difference rates. At the aggregate level, the point-source approximation substantially underestimates damage, predicting approximately 24,385 completely damaged buildings (73% difference rate). In contrast, the planar and pre-calculated rupture models yield significantly more accurate estimates (82,258 and 99,060 buildings, respectively), both with difference rates of just 9% compared to the complex rupture model reference. Provincial-level analysis demonstrates even more pronounced effects of rupture model sophistication. The point-source approximation shows particularly poor performance in heavily affected provinces, with difference rates of 69% (Kahramanmaraş), 97% (Hatay), and 28% (Gaziantep). These discrepancies dramatically improve when using the pre-calculated rupture model, with corresponding difference rates falling to 9%, 22%, and 4%, respectively. Consistent with other loss metrics, the pre-calculated rupture model demonstrates superior overall accuracy, achieving the lowest aggregate discrepancy (16%) among all approximate methods.

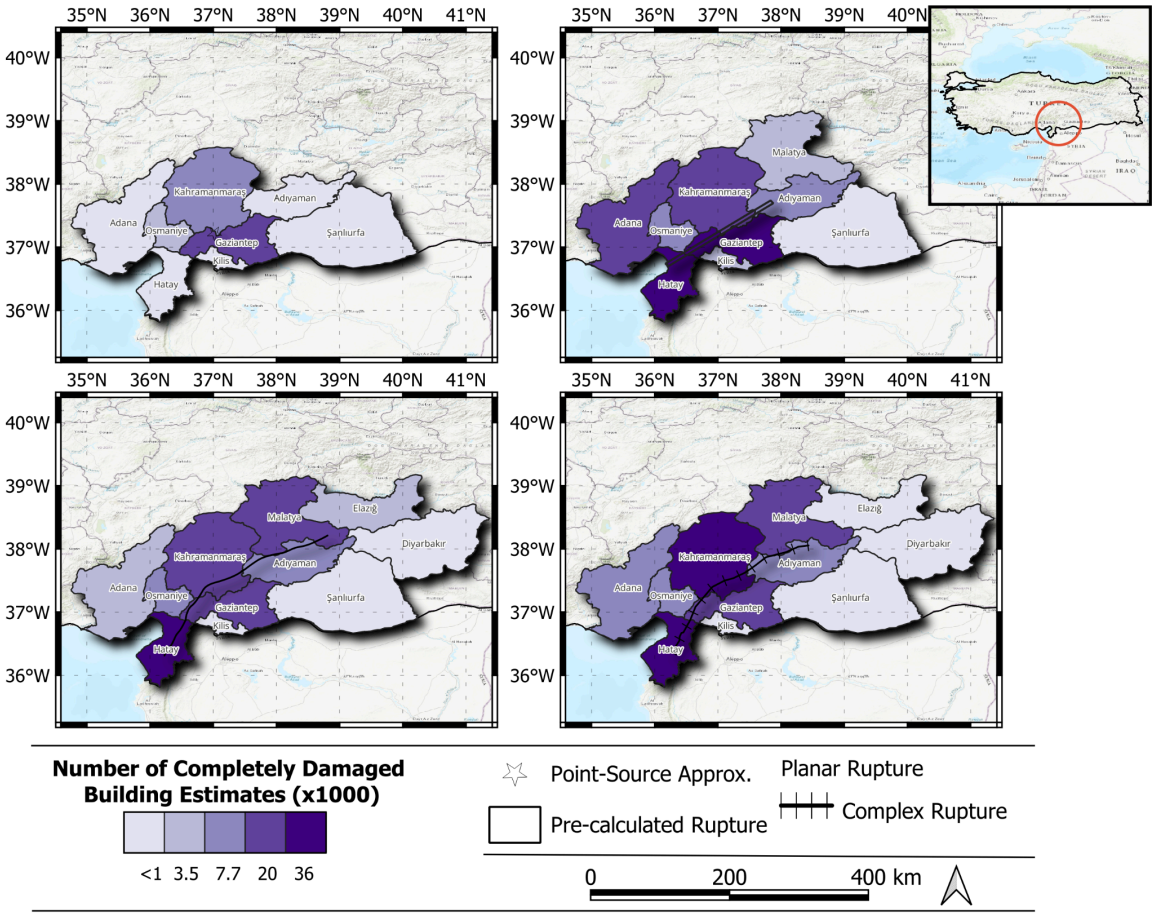

Figure 7. Spatial distribution of the number of completely damaged buildings estimates obtained by each rupture modeling approach for the Kahramanmaras earthquake example.

Table 7. Mean number of completely damaged buildings estimates disaggregated by province for each rupture modeling approach in the Kahramanmaras earthquake example.

Province	Number of Completely Damaged Buildings Estimates			
	Point-Source	Planar	Pre-Calculated	Complex Finite
ADANA	82 (98%)	12,412 (188%)	3,544 (18%)	4,303
ADIYAMAN	204 (97%)	5,723 (23%)	7,711 (4%)	7,439
DIYARBAKIR	-	-	401 (488%)	68
ELAZIG	-	-	2,588 (252%)	736
GAZIANTEP	13,664 (28%)	19,735 (84%)	10,257 (4%)	10,712
HATAY	833 (97%)	23,498 (20%)	35,768 (22%)	29,243
K.MARAS	6,445 (69%)	9,214 (56%)	19,072 (9%)	20,984
KILIS	724 (15%)	1,066 (26%)	834 (2%)	848
MALATYA	1 (100%)	2,795 (73%)	10,765 (4%)	10,319
OSMANIYE	2,305 (56%)	6,804 (31%)	7,069 (36%)	5,184
SANLIURFA	127 (84%)	1,010 (27%)	1,052 (32%)	796
Total	**24,385 (73%)**	**82,258 (9%)**	**99,060 (9%)**	**90,632**
Weighted Regional Difference	**80%**	**52%**	**16%**	-

c. 2016 M7.0 Kumamoto, Japan Earthquake

On April 16, 2016, a devastating M_w = 7.0 earthquake struck the Kumamoto Prefecture in western Japan. This shallow crustal event, occurring at a depth of 9 km, resulted from strike-slip faulting within the Eurasian plate. Official reports from the Asian Disaster Reduction Center (ADRC, 2016) documented severe consequences: 228 fatalities, 2,753 injuries (including 1,400 serious cases), and widespread structural damage affecting approximately 190,000 buildings - 8,697 of which completely collapsed. The earthquake also triggered significant secondary hazards, including landslides, debris flows, and slope failures. This study examines the Kumamoto earthquake as a representative case of a major seismic event affecting densely populated regions.

i. PGA estimates for the Kumamoto earthquake example

Figure 8 presents the PGA estimates for each rupture model using exclusively the GMM developed by Zhou et al. (2016). The point-source approximation, as anticipated, produced the most constrained shaking distribution, with peak PGA values ranging between 0.40g and 0.62g across a limited area. When more detailed rupture geometries with specific orientations are incorporated, the affected region shows substantial changes. The planar rupture model demonstrates a pronounced expansion of the impact area experiencing PGAs from 0.40g to 0.62g. While less extensive than the planar rupture model, the pre-calculated rupture model still exhibits a broader spatial distribution of peak PGA estimates compared to the point-source approximation. Most notably, the complex rupture model, which incorporates the most detailed geometry, generates both a distinct spatial pattern and significantly higher PGA values ranging from 0.62g to 0.86g

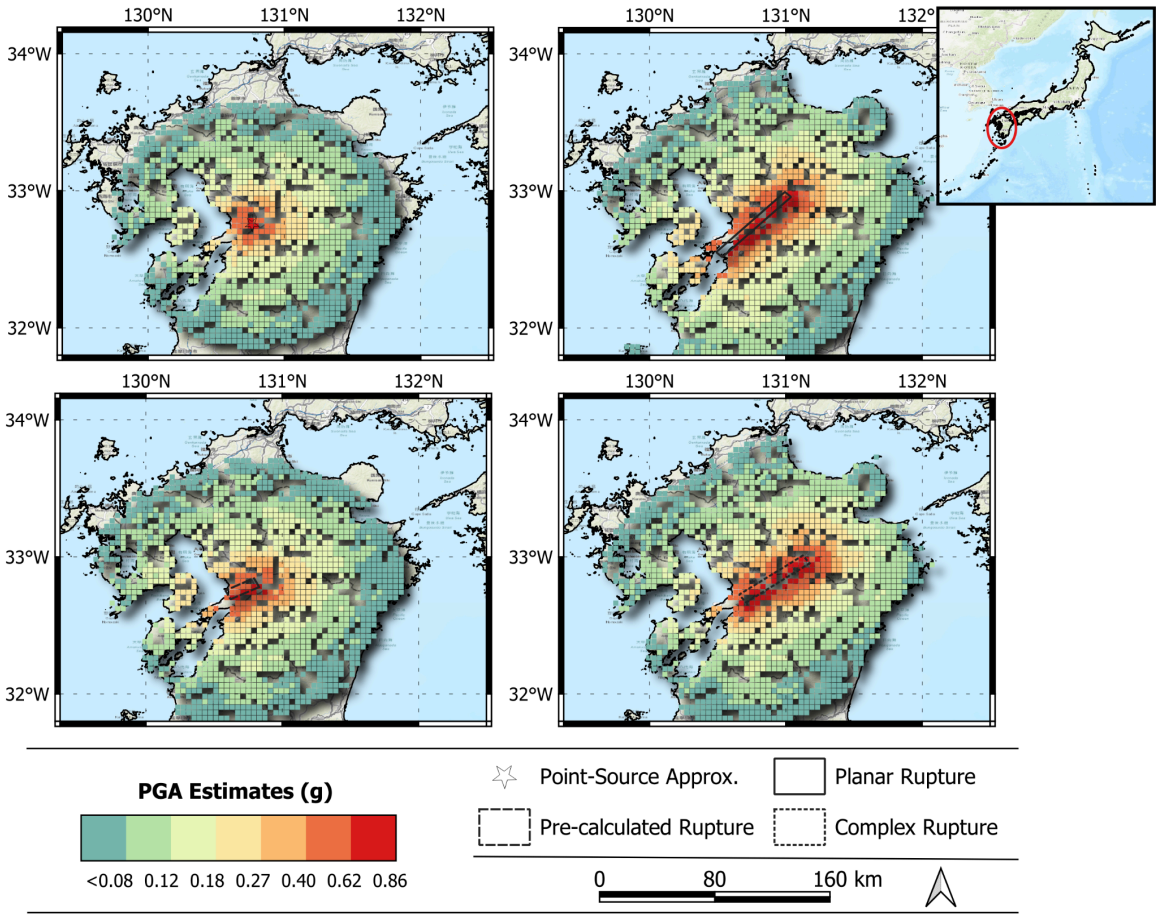

Figure 8. The spatial distribution of PGA estimates for each rupture modeling approach for the Kumamoto earthquake example.

ii. Economic loss estimates for the Kumamoto earthquake example

Figure 9 presents the spatial distribution of economic loss estimates derived from different rupture modeling approaches for the Kumamoto earthquake scenario. Kumamoto Prefecture consistently emerges as the most severely affected region across all modeling approaches. Notably, Fukuoka Prefecture also shows substantial economic losses when using larger rupture geometries (planar, pre-calculated, and complex), reflecting the expanded impact area predicted by these approaches. Table 8 summarizes the economic loss estimates and their corresponding difference rates relative to the complex rupture model, presenting both aggregate and prefecture-level results. At the national level, the point-source approximation substantially underestimates losses (≈$14.0 billion; 20% difference rate), while the planar ($20.8 billion; 20%) and pre-calculated ($18.9 billion; 9%) models show improved accuracy. As for the prefecture-level analysis, while the point-source and planar models show similar aggregate difference rates (≈20%), the pre-calculated rupture model achieves superior accuracy with just 13% discrepancy overall.

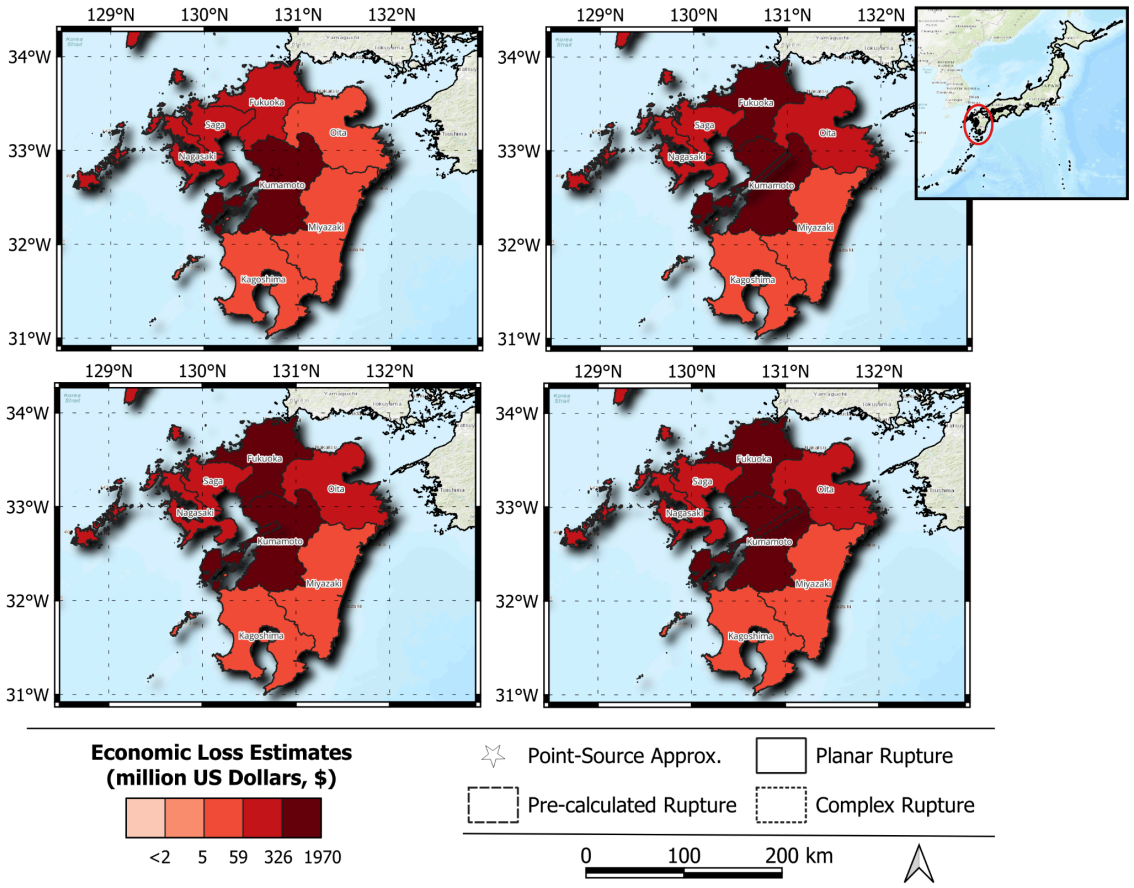

Figure 9. The spatial distribution of economic loss estimates for each rupture modeling approach for the Kumamoto earthquake example.

Table 8. Mean economic loss estimates disaggregated by prefecture for each rupture modeling approach for the Kumamoto earthquake example.

Prefecture	Economic Loss Estimates (Million US Dollars)			
	Point-Source	Planar	Pre-Calculated	Complex Finite
Fukuoka	304.8 (23%)	536.3 (36%)	464.5 (18%)	394.3
Kagoshima	5.2 (29%)	48.3 (558%)	8.7 (18%)	7.3
Kumamoto	13,440.3 (18%)	19,627.7 (20%)	17,968.5 (10%)	16,340.1
Miyazaki	25.3 (51%)	48.9 (5%)	30.4 (41%)	51.7
Nagasaki	91.1 (21%)	231.5 (100%)	235.4 (103%)	115.7
Oita	56.0 (87%)	265.0 (37%)	87.3 (79%)	422.4
Saga	69.7 (4%)	81.5 (22%)	106.3 (59%)	66.7
TOTAL	**13,992.3 (20%)**	**20,839.1 (20%)**	**18,901.1 (9%)**	**17,398.2**
Weighted Regional Diff.	**20%**	**22%**	**13%**	-

iii. Fatality estimates for the Kumamoto earthquake example

Table 9 summarizes fatality estimates and corresponding difference rates for each rupture model at both aggregate and prefecture levels. At the aggregate level, the point-source approximation yields the closest estimate (≈85 fatalities; 3% difference rate), while the planar (105; 19%) and pre-calculated (109; 25%) models show progressively larger discrepancies relative to the complex rupture model reference. Kumamoto Prefecture dominates the national fatality estimates across all models. As a comparison on the prefecture level, the point-source approximation achieves remarkable accuracy in Kumamoto (1% difference), whereas the planar (19%) and pre-calculated (26%) models exhibit substantially larger discrepancies.

Table 9. Mean number of fatality estimates disaggregated by prefecture for each rupture modeling approach in the Kumamoto earthquake example.

Prefecture	Number of Fatality Estimates (person)			
	Point-Source	Planar	Pre-Calculated	Complex Finite
Fukuoka	1 (24%)	2 (46%)	2 (30%)	1
Kumamoto	84 (1%)	102 (19%)	107 (26%)	85
Oita	-	1 (33%)	-	1
Total	**85 (3%)**	**105 (19%)**	**109 (25%)**	**87**
Weighted Regional Difference	**3%**	**20%**	**27%**	**-**

iv. Number of completely damaged buildings estimates for the Kumamoto earthquake example

Figure 10 illustrates the spatial distribution of the estimated number of completely damaged buildings across different rupture modeling approaches. Table 10 complements this visualization by presenting both aggregate and prefecture-level estimates along with their corresponding difference rates. At the aggregate level, the point-source approximation estimates approximately 19,450 completely damaged buildings (24% difference rate). The planar and pre-calculated rupture models yield higher estimates of 31,540 (23%) and 26,890 (4%) buildings, respectively. Consistent with other loss metrics for this event, the Kumamoto Prefecture dominates the total damage estimates, making prefecture-level analysis particularly valuable for drawing comprehensive conclusions. When examining Kumamoto specifically, both the point-source approximation (19,260 buildings) and planar rupture model (30,980 buildings) show similar difference rates of 23%. In contrast, the pre-calculated rupture model demonstrates significantly better agreement with the reference data, estimating 26,460 completely damaged buildings with just a 5% difference rate.

Table 10. Mean number of completely damaged building estimates disaggregated by prefecture for each rupture modeling approach in the Kumamoto earthquake example.

Prefecture	Number of Completely Damaged Buildings Estimates			
	Point-Source	Planar	Pre-Calculated	Complex Finite
Fukuoka	103 (0%)	167 (62%)	171 (66%)	103
Kagoshima	2 (37%)	24 (805%)	4 (42%)	3
Kumamoto	19,259 (23%)	30,978 (23%)	26,459 (5%)	25,165
Miyazaki	9 (71%)	23 (21%)	12 (61%)	30
Nagasaki	49 (25%)	180 (173%)	188 (185%)	66
Oita	13 (96%)	144 (60%)	22 (94%)	363
Saga	19 (18%)	23 (44%)	33 (111%)	16
TOTAL	**19,453 (24%)**	**31,540 (23%)**	**26,889 (4%)**	**25,745**
Weighted Regional Difference	**24%**	**24%**	**7%**	**-**

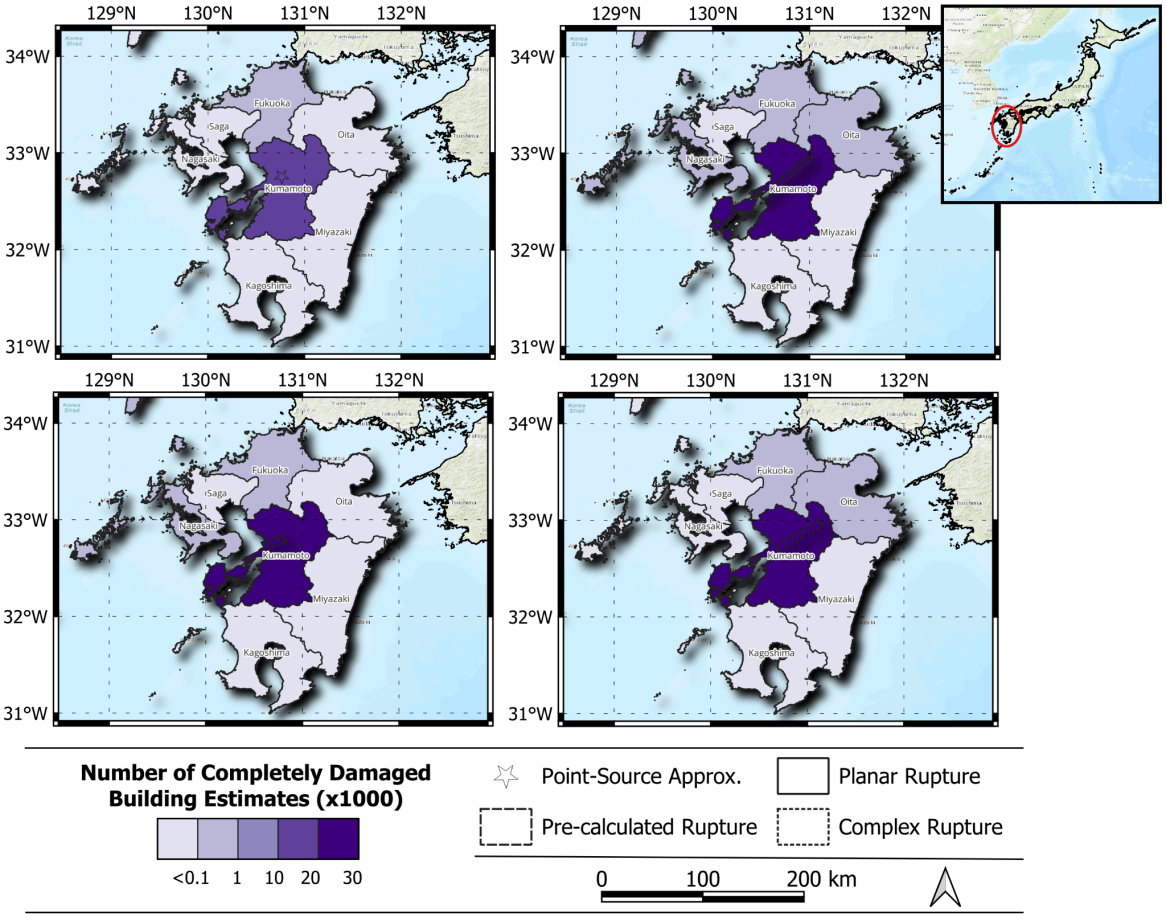

Figure 10. The spatial distribution of the number of completely damaged buildings estimates obtained by each rupture modeling approach for the Kumamoto earthquake example.

d. 2009 M6.3 L'Aquila, Italy Earthquake

On April 6, 2009, an earthquake with a magnitude of M_w = 6.3 struck central Italy's Apennine region through normal faulting mechanisms, with its epicenter near L'Aquila. The seismic event caused catastrophic damage to this medieval city and surrounding areas, resulting in 308 fatalities and displacing 67,500 residents (Volpini, 2009). The structural damage assessments revealed extensive damage to approximately 60,000 buildings, including vulnerable historical structures, critical hospitals, and essential infrastructure in the ancient city of L'Aquila (Casarotti et al. 2009). Despite its moderate magnitude, the earthquake's severe impacts - amplified by the region's high seismic vulnerability and concentration of historic masonry buildings and this event is considered a classical example demonstrating a medium-magnitude earthquake (Alexander D. E., 2010).

i. PGA estimates for the L'Aquila earthquake example

Figure 11 presents the peak ground acceleration (PGA) estimates for each rupture model using exclusively the GMM developed by Bindi et al. (2016). Unlike the other studied earthquakes, the L'Aquila event shows relatively minor variations in PGA spatial distribution across rupture models, consistent with its moderate magnitude (M_w 6.3). The impact area remains largely confined to the epicentral region regardless of modeling approach. The point-source approximation produces high PGAs (0.25g-0.43g) strictly at the epicenter, while the planar and pre-calculated rupture models extend this intensity range over a slightly broader area through their specific rupture geometries. The complex rupture model also generates a similar PGA distribution pattern to the other approximated approaches, except that it predicts higher PGAs (0.43g–0.65g) affecting an extended region beyond the immediate epicenter.

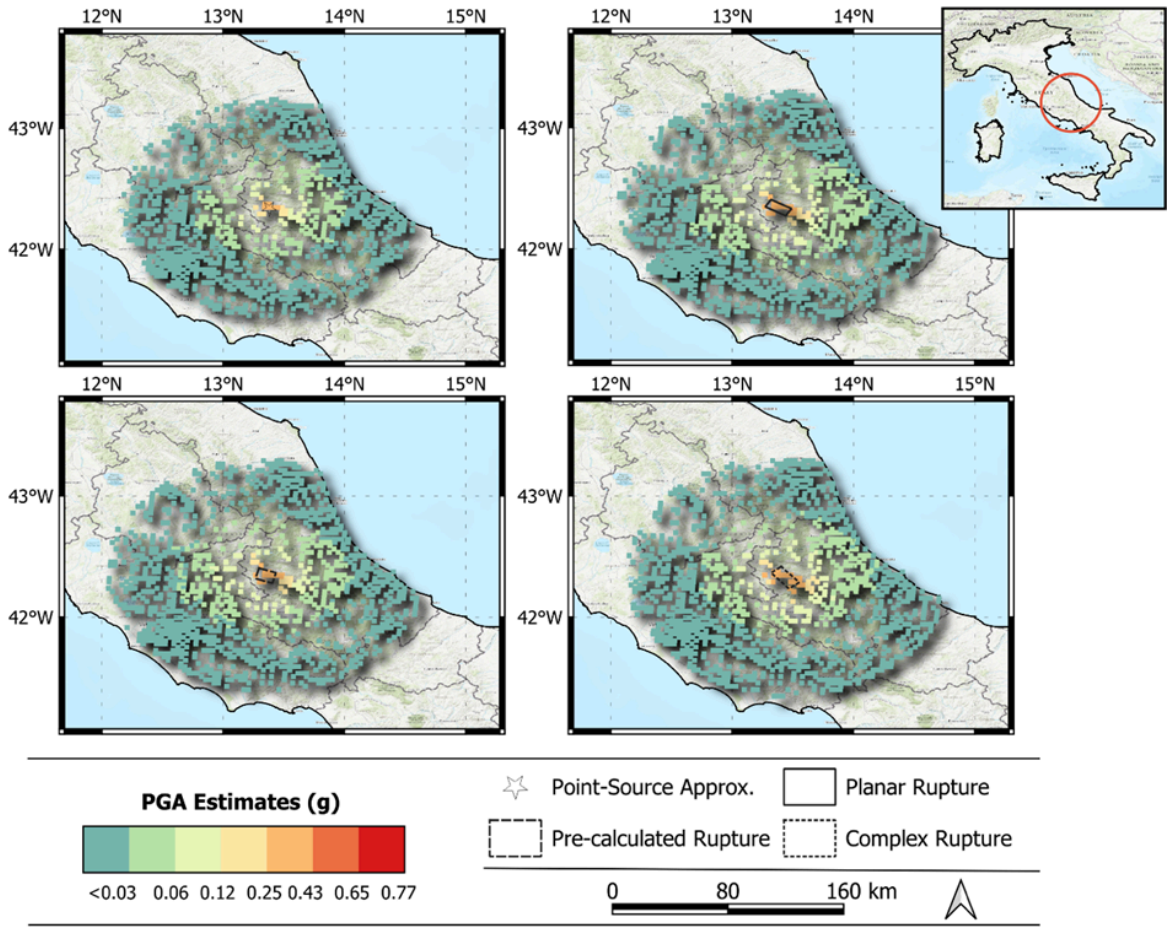

Figure 11. The spatial distribution of PGA estimates for each rupture modeling approach for the L'Aquila earthquake example.

ii. Economic loss estimates for the L'Aquila earthquake example

Figure 12 presents the spatial distribution of economic loss estimates across different rupture modeling approaches for the L'Aquila earthquake. Consistent with the ground shaking patterns, all models show the highest economic losses concentrated in the Abruzzo region. The point-source, planar, and pre-calculated rupture models produce particularly well-aligned loss estimates with that of the complex rupture model in this area. More importantly, the analysis reveals that the planar and pre-calculated rupture models generate spatial loss distributions that closely match the complex rupture model's results throughout most of the study area. The only notable difference occurs in Molise, where these simplified models show less agreement with the complex rupture model.

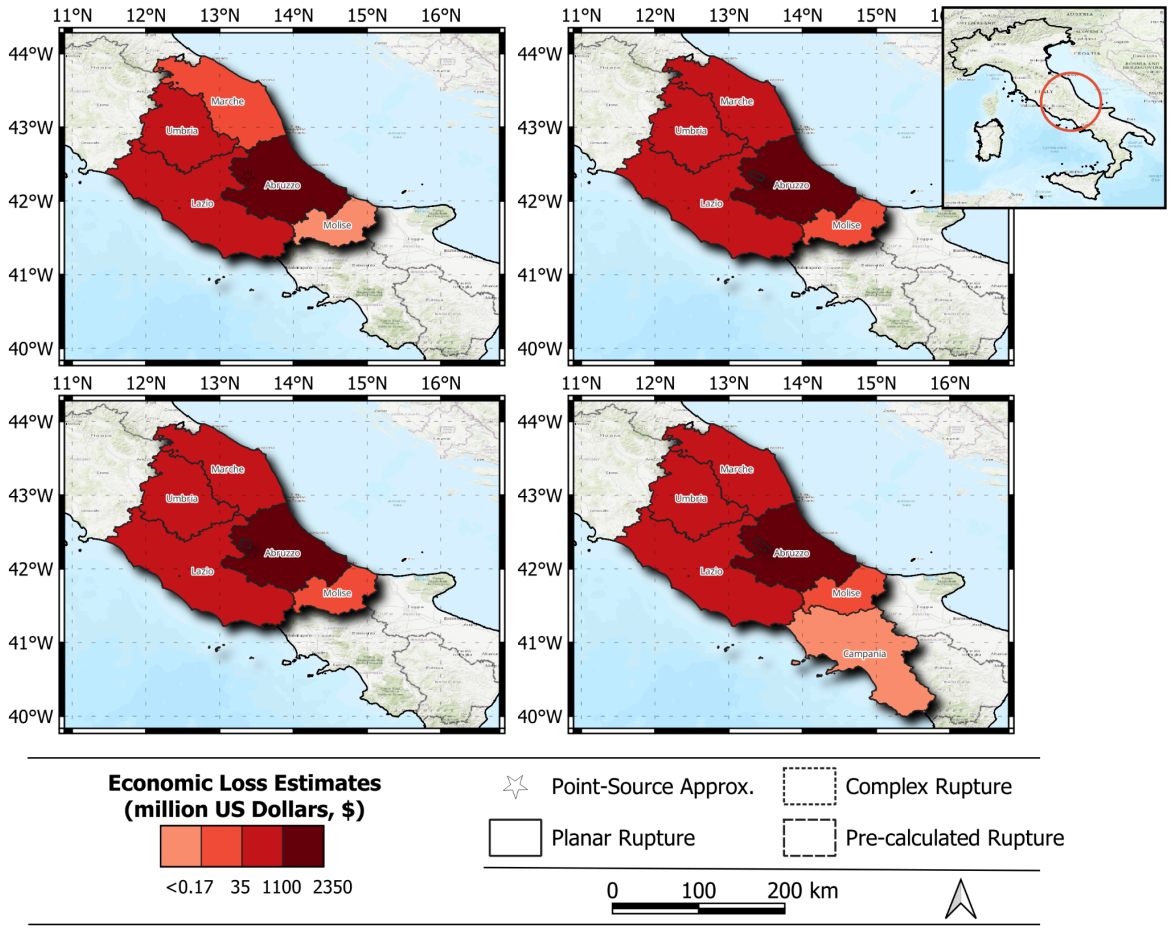

Figure 12. The spatial distribution of economic loss estimates for each rupture modeling approach for the L'Aquila earthquake example.

Table 11 summarizes the economic loss estimates and corresponding difference rates for each rupture model at both the aggregate and regional levels. At the aggregate level, the point-source approximation yields the lowest economic loss estimate (~$1.7 billion) and shows the highest discrepancy (39% difference rate). In contrast, the planar and pre-calculated rupture models provide more accurate estimates of $2.7 billion (6% difference) and $2.4 billion (13% difference), respectively. However, the regional analysis reveals important variations in model performance. While the planar rupture model maintains relatively good accuracy (11% difference rate across all regions), the pre-calculated model's discrepancy increases to 21%. The point-source approximation remains the least accurate approach at both spatial scales.

Table 11. Mean economic loss estimates disaggregated by region for each rupture modeling approach for the L'Aquila earthquake example.

Region	Economic Loss Estimates (Million US Dollars)			
	Point-Source	Planar	Pre-Calculated	Complex Finite
Abruzzo	1,305.9 (44%)	2,091.6 million (10%)	1,848.1 (20%)	2,323.5
Campania	-	-	-	0.1
Lazio	372.8 (17%)	526.7 (17%)	541.6 (20%)	451.8
Marche	27.3 (44%)	37.8 (23%)	35.3 (28%)	48.9
Molise	0.1 (93%)	0.3 (74%)	0.2 (83%)	1.3
Umbria	41.2 (26%)	66.0 (19%)	75.5 (36%)	55.4
Total	**1,747.3 (39%)**	**2,722.5 (6%)**	**2,500.6 (13%)**	**2,881.0**
Weighted Regional Difference	**39%**	**11%**	**21%**	**-**

iii. Fatality estimates for the L'Aquila earthquake example

Table 12 presents the number of fatality estimates and corresponding difference rates for each rupture model at both the aggregate and regional levels. At the aggregate level, the point-source approximation significantly underestimates fatalities (74; 49% difference rate), while the planar (135; 8%) and pre-calculated (121; 17%) models show substantially better agreement with the complex rupture model reference. The analysis reveals that the Abruzzo region accounts for the majority of estimated fatalities across all models. The region-level results demonstrate particularly poor performance of the point-source approximation (49% difference rate) and pre-calculated model (19%), while the planar rupture model maintains strong accuracy (8% difference rate) in this most affected region.

Table 12. Mean number of fatality estimates disaggregated by region for each rupture modeling approach in the L'Aquila earthquake example.

Region	Number of Fatality Estimates (person)			
	Point-Source	Planar	Pre-Calculated	Complex Finite
Abruzzo	73 (49%)	131 (8%)	117 (19%)	144
Lazio	1 (42%)	3 (44%)	4 (80%)	2
Total	**74 (49%)**	**135 (8%)**	**121 (17%)**	**146**
Weighted Regional Difference	**49%**	**9%**	**20%**	**-**

iv. Number of completely damaged buildings estimates for the L'Aquila earthquake example

Figure 13 presents the spatial distribution of completely damaged building estimates across different rupture modeling approaches, providing a key visualization of this critical loss metric. Table 13 complements this spatial analysis by presenting quantitative estimates and corresponding difference rates at both aggregate and region levels. The point-source approximation yields a national estimate of approximately 2,000 completely damaged buildings, showing a substantial discrepancy (53% difference rate). In contrast, more sophisticated approaches demonstrate improved accuracy: the planar rupture model estimates 3,939 buildings (7% difference rate), while the pre-calculated model predicts 3,518 buildings (17% difference rate). When examining regional results, the point-source approximation maintains its high discrepancy (53%), while the planar and pre-calculated rupture models show slightly increased difference rates of 9% and 21% respectively.

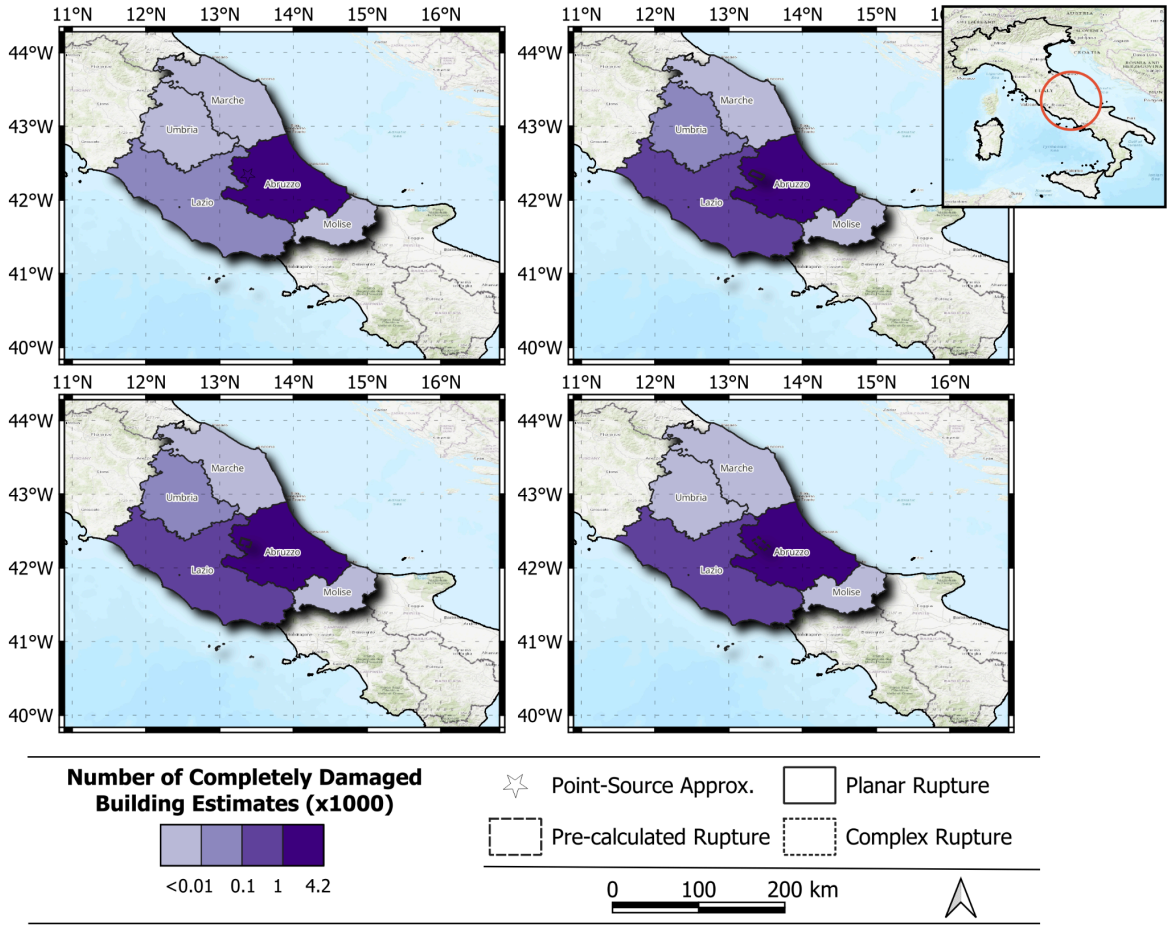

Figure 13. The spatial distribution of the number of completely damaged buildings estimates obtained by each rupture modeling approach for the L'Aquila earthquake example.

Table 13. Mean number of completely damaged building estimates disaggregated by region for each rupture modeling approach in the L'Aquila earthquake example.

Region	Number of Completely Damaged Buildings Estimates			
	Point-Source	Planar	Pre-Calculated	Complex Finite
Abruzzo	1,931 (53%)	3,781 (8%)	3,324 (19%)	4,111
Lazio	61 (39%)	144 (43%)	178 (77%)	101
Marche	2 (65%)	3 (35%)	3 (47%)	5
Umbria	5 (44%)	10 (26%)	13 (62%)	8
TOTAL	**1,998 (53%)**	**3,939 (7%)**	**3,518 (17%)**	**4,225**
Weighted Regional Difference	**53%**	**9%**	**21%**	-

e. 2011 M5.1 Lorca, Spain Earthquake

On May 11, 2011, a moderate M_w = 5.1 earthquake struck the city of Lorca in Spain's Murcia region. This shallow crustal event (depth = 1 km) occurred along the Eurasian-African plate boundary, likely associated with strike-slip motion on a secondary fault near the major Alhama de Murcia fault system (USGS, 2011). The exceptionally shallow hypocentral depth led to observable surface rupture near the fault trace (EFE, 2011). Despite its moderate magnitude, the earthquake caused significant impacts: 9 fatalities, 403 injuries, and extensive damage to masonry structures, including partial collapses (Hermanns et al., 2014). Notably, this event represents the third strongest earthquake recorded by strong-motion instruments in Spain since 1951. Unlike other case studies, we excluded the pre-calculated rupture model for Lorca since the available fault sources in the seismic hazard model adopted in this study cannot adequately represent such low-magnitude events.

i. PGA estimates for the Lorca earthquake example

Figure 14 presents the PGA estimates for each rupture model using exclusively the GMM developed by Cauzzi et al. (2014). The Lorca earthquake (M_w 5.1) results in limited variability in ground shaking patterns across different rupture models. Both the point-source approximation and planar rupture model produce nearly identical PGA distributions (0.02g - 0.55g), with similar spatial extents of ground shaking concentrated near the epicenter. The complex rupture model, while incorporating more detailed fault geometry, yields a PGA distribution pattern largely consistent with the simpler models, showing only minor variations in intensity values. This remarkable consistency across modeling approaches highlights how rupture geometry exerts a relatively minor influence on ground shaking estimates for moderate-magnitude events, providing important insights for seismic hazard assessment of similar earthquakes.

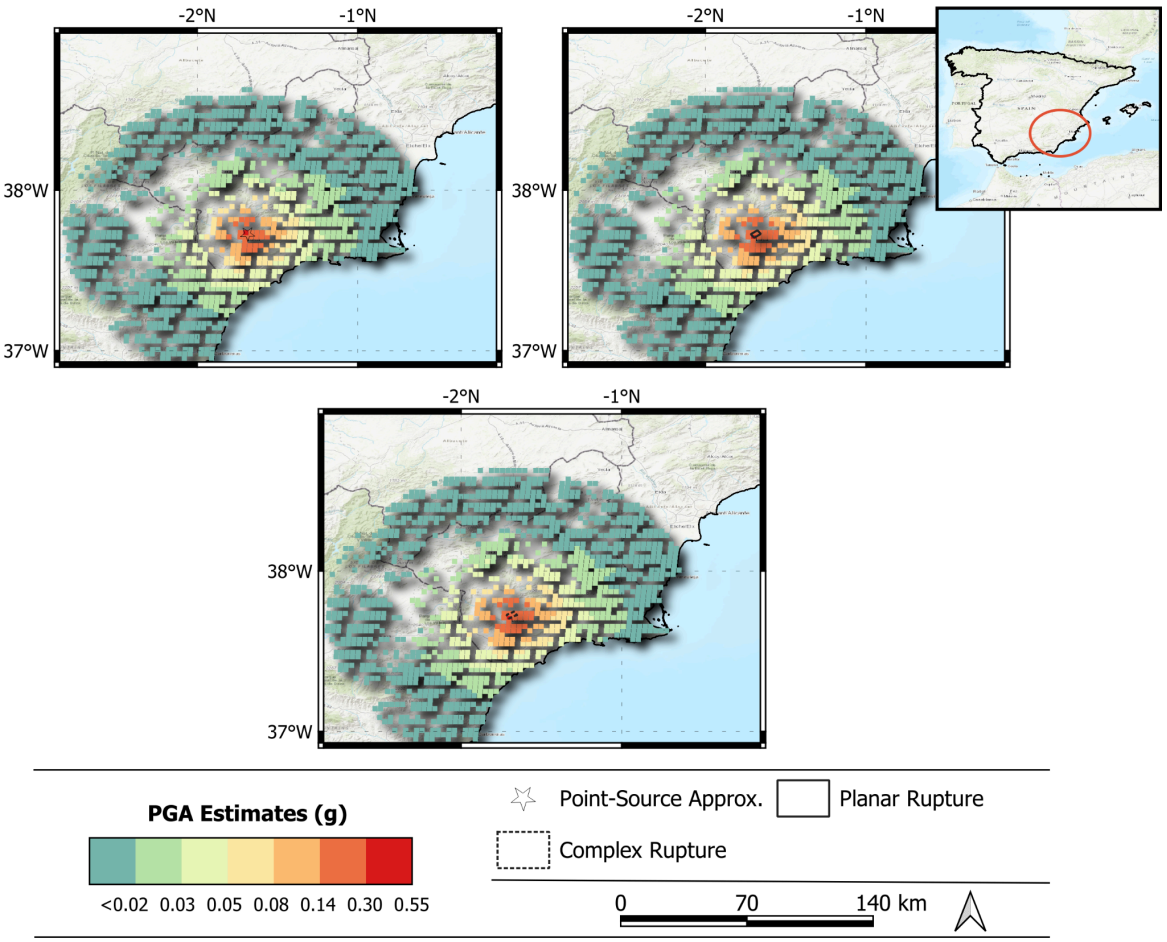

Figure 14. The spatial distribution of PGA estimates for each rupture modeling approach for the Lorca earthquake example.

ii. Economic loss estimates for the Lorca earthquake example

The spatial distribution of economic losses for the Lorca earthquake, as depicted in Figure 15, reveals key insights across the different rupture modeling approaches. The Region of Murcia consistently emerges as the region with the highest economic losses in all rupture models. While the planar and complex rupture models produce similar spatial distributions of estimated losses, the point-source approximation tends to slightly underestimate them, particularly within the epicentral region. Notably, economic loss estimates remain largely consistent across most regions, with significant variation only observed near the epicenter. These results underscore that even for low-magnitude earthquakes, the choice of rupture geometry influences impact assessments, especially in the epicentral region.

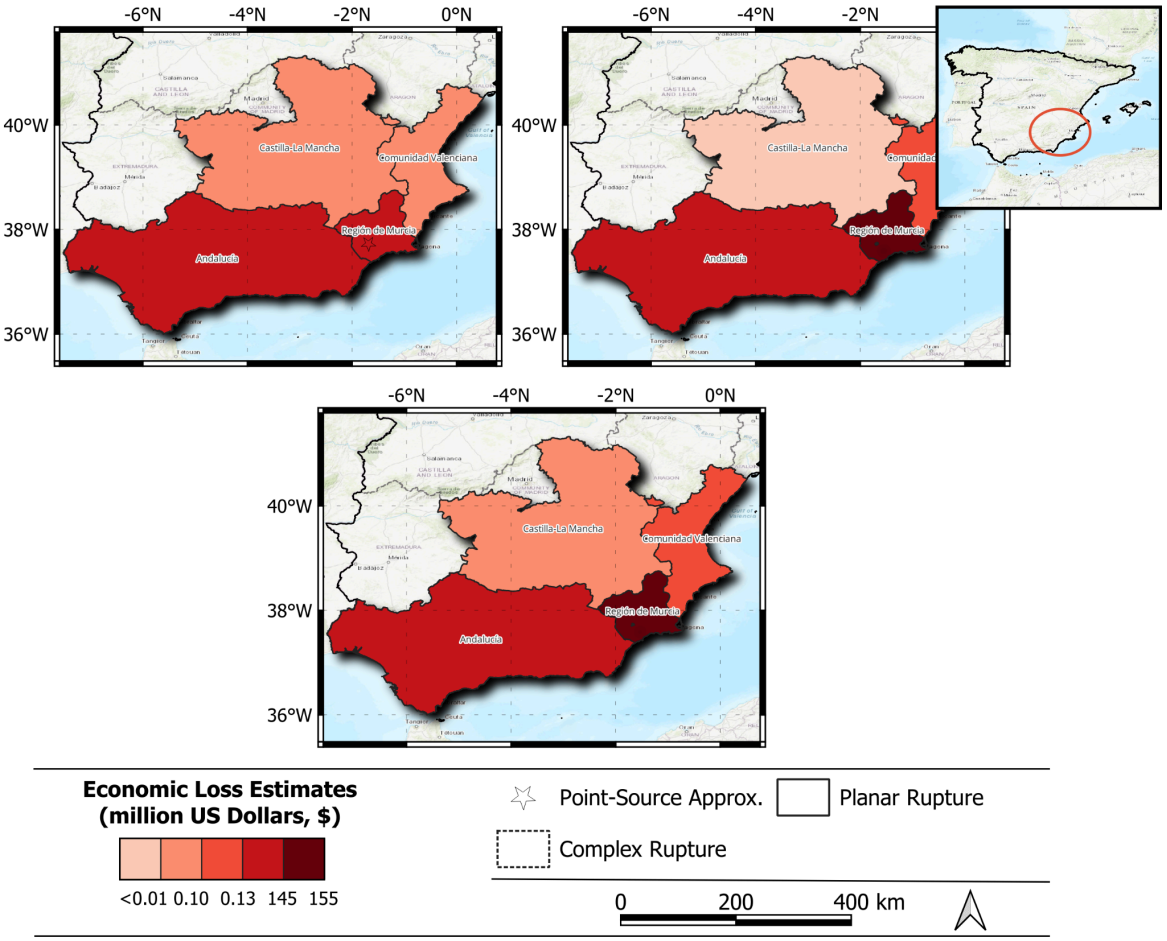

Figure 15. The spatial distribution of economic loss estimates for each rupture modeling approach for the Lorca earthquake example.

Table 14 summarizes the economic loss estimates and their corresponding difference rates at both the aggregate and regional levels for each rupture model. At the aggregate level, the complex rupture model yields an estimated loss of approximately 155 million USD, whereas the point-source and planar rupture models produce lower estimates of around 96 million USD and 147 million USD, respectively. These figures correspond to difference rates of 38% and 5% when compared to the complex rupture model. A more detailed regional analysis reveals that the spatial distribution of losses and difference rates aligns with the aggregated results, particularly in the Region de Murcia, due to the influence of the event's low magnitude.

Table 14. Mean economic loss estimates disaggregated by region for each rupture modeling approach for the Lorca earthquake example.

Region	Economic Loss Estimates (Million US Dollars)		
	Point-Source	Planar	Complex Finite
Andalucia	0.3 (23%)	0.4 (3%)	0.4
Castilla-La Mancha	0.01 (8%)	0.01 (24%)	0.01
Comunidad Valenciana	0.1 (23%)	0.1 (14%)	0.1
Region de Murcia	95.9 (38%)	146.0 (5%)	154.2
TOTAL	**96.3 (38%)**	**146.5 (5%)**	**154.8**
Weighted Regional Difference	**38%**	**5%**	-

iii. Fatality estimates for the Lorca earthquake example

Table 15 summarizes the fatality estimates and corresponding difference rates for each rupture model, focusing solely on the Region de Murcia, as other affected areas are projected to have negligible fatalities (fewer than 1). As shown in the table, the complex rupture model estimates approximately 6 fatalities, while the point-source and planar rupture models yield lower estimates of around 3 and 5 fatalities, respectively. These figures correspond to difference rates of 49% and 6% compared to the complex rupture model.

Table 15. Mean number of fatality estimates disaggregated by region for each rupture modeling approach in the Lorca earthquake scenario.

Region	Number of Fatality Estimates (person)		
	Point-Source	Planar	Complex Finite
Region de Murcia	3 (49%)	5 (6%)	6

iv. Number of completely damaged buildings estimates for the Lorca earthquake example

Figure 16 illustrates the spatial distribution of the estimated number of completely damaged buildings across each rupture modeling approach. Table 16 further quantifies these estimates, presenting the total number of completely damaged buildings and corresponding difference rates for each rupture modeling approach. According to these results, the complex rupture model predicts approximately 230 completely damaged structures. In contrast, the point-source and planar rupture models yield significantly lower estimates of 126 and 219 buildings, representing difference rates of 45% and 5%, respectively, compared to the complex rupture model.

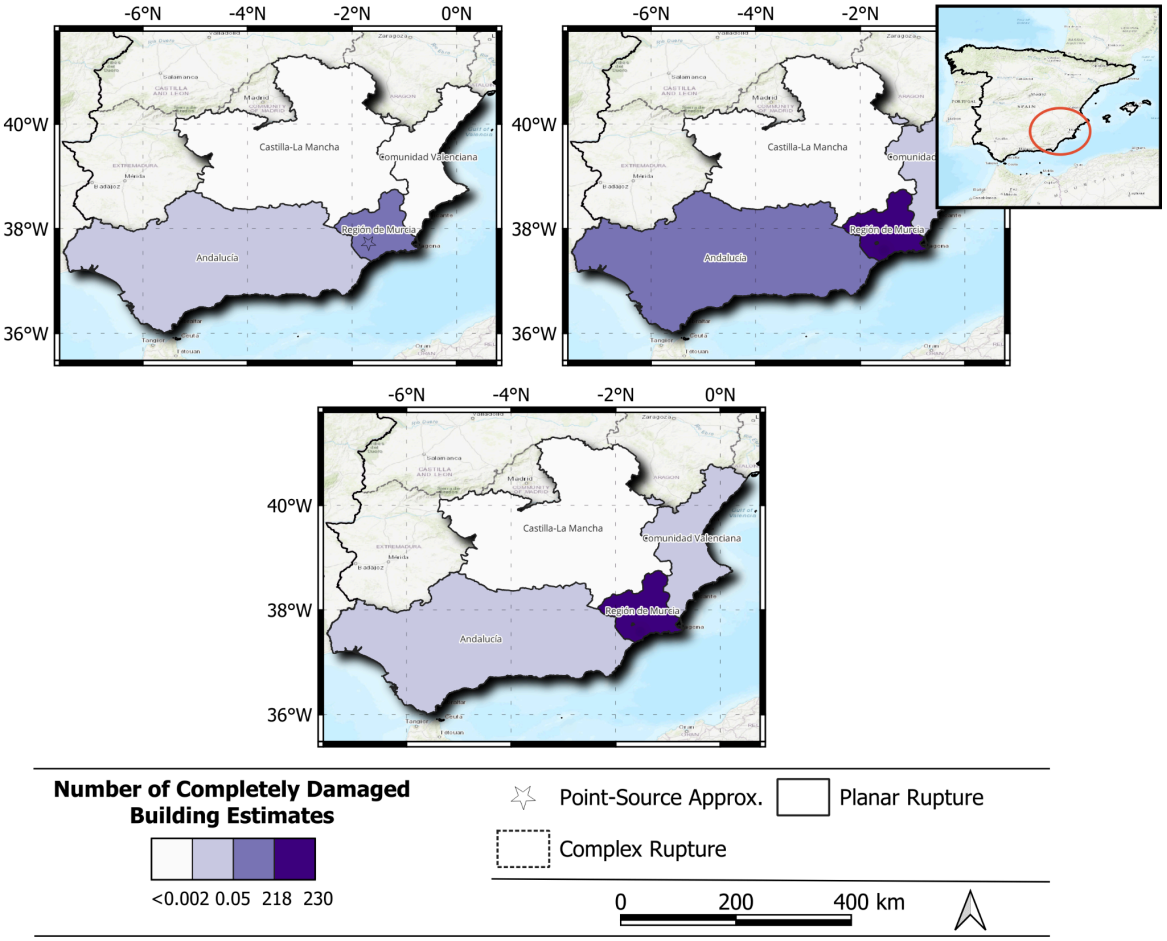

Figure 16. The spatial distribution of the number of completely damaged buildings estimates obtained by each rupture modeling approach for the Lorca earthquake example.

Table 16. Mean number of completely damaged buildings estimates disaggregated by region for each rupture modeling approach in the Lorca earthquake example.

Region	Number of Completely Damaged Buildings Estimates		
	Point-Source	Planar	Complex Finite
Region de Murcia	126 (45%)	219 (5%)	230

6. Discussion of the results

The impact analyses conducted in this study are predicated on the assumption that the exposure and vulnerability components are sufficiently accurate. However, as noted in prior research (e.g., Villar and Silva 2017), exposure and vulnerability models are often subject to incompleteness, bias, and/or out-of-date data, which can substantially influence impact estimates. In many cases, these uncertainties introduce greater deviations than those attributable to the rupture modeling approaches examined in this study.

The approximation of earthquake rupture as a point source consistently resulted in an underestimation of impact. Nevertheless, discernible patterns emerged across real-world events, suggesting that these systematic biases may be amenable to correction via adjustment factors. It is reasonable to assume that for small to moderate magnitude events (M<6), damages and losses can be expected to be 25 to 50% higher, while for stronger events (M>6), the impact can be expected to be 50 to 100% higher if the rupture geometry is approximated to a point-source.

The planar rupture modeling approach—a feasible solution within the first hour following an event—yielded reasonably accurate impact estimates, particularly when assessing aggregate impacts (deviations remained below 25% relative to benchmark results). However, its performance proved less reliable at the regional level, as evidenced by the weighted regional difference parameter. This limitation was particularly pronounced in the case of the 2023 M7.8 Kahramanmaraş earthquake, where the benchmark rupture deviated substantially from a planar geometry. Additionally, a critical constraint of this method lies in the inherent uncertainty of nodal plane selection: since two potential fault plane solutions are typically available, identifying the one most closely aligned with the actual rupture remains challenging, especially in regions with poorly characterized fault systems.

The pre-calculated rupture model, derived primarily from probabilistic seismic hazard assessments, demonstrated consistent efficacy in estimating a range of risk metrics at both aggregated and provincial/regional scales. Although this approach does not constrain rupture geometry with the same precision as finite-fault models, which incorporate seismic waveform inversion and geodetic observations, it nevertheless yielded more reliable impact estimates than the point-source approximation and even than planar rupture when estimates across all regions are considered. These findings underscore the practical value of pre-calculated rupture models as a viable alternative to point-source representations in scenarios requiring rapid post-event impact assessment, particularly when the finite-fault solutions are unavailable.

7. Conclusions

This study comprehensively examined the influence of varying rupture geometry identification methods on rapid earthquake impact assessment results, focusing on both the ground shaking estimates and various risk metrics: economic losses, number of fatalities and the number of completely damaged buildings. The scenario-based risk analyses conducted for the earthquake examples covered a broad range of event characteristics, including varying magnitudes, rupture geometries, and spatial distributions of the asset. These analyses were performed using the OpenQuake Engine, an open-source platform developed by the Global Earthquake Model (GEM) initiative, integrating region-specific hazard, exposure, and vulnerability models. At the end, we compared the ground shaking and impact estimates from three simplified rupture modeling approaches against a reference rupture geometry assumed to closely represent the actual seismic event. To quantitatively assess the influence of rupture geometry, the percent difference and weighted regional difference of the rupture models were calculated.

The findings from the impact assessments for each earthquake scenario are summarized as follows:

- Moderate-magnitude seismic events (M < 6.0) with epicentral distances exceeding 30 km from populated areas can be accurately represented using a simplified point-source approximation with minimum impact on accuracy.
- For seismic events occurring near or directly beneath urban centers, detailed finite-rupture modeling is essential, irrespective of magnitude. The analysis results indicate that point-source approximation systematically underestimates impacts, with discrepancies reaching ~50% for moderate events (M < 6.0) and up to a factor of 2 for stronger earthquakes.
- Planar rupture models, when constrained by a single nodal plane, generally produce acceptable results (impact deviations <25% relative to benchmark solutions). However, their reliability depends critically on the correct identification of the causative fault plane, ideally supported by national or global active fault databases.
- In regions characterized by arcuate or non-planar fault geometries (e.g., the Middle America Trench, North Panama Deformed Belt, Cyprus–Türkiye fault system, and Xiangshihe–Xiaojiang Fault; Styron and Pagani, 2020), planar rupture models exhibit reduced accuracy, particularly at subnational scales where fault curvature effects become pronounced.
- Pre-calculated rupture models derived from probabilistic seismic hazard analysis (PSHA) can significantly improve impact estimates in tectonically complex regions. However,

their efficacy is contingent upon the underlying fault characterization accuracy. Even in well-studied areas, observed ruptures (e.g., the 2016 M7.8 Kaikōura earthquake or the 2025 M7.7 Myanmar event) may exhibit substantial deviations from modeled scenarios due to multi-fault triggering or off-fault deformation.

- For small-to-moderate events (M < 6.0), the pre-calculated ruptures offer limited practical utility, as such seismicity is typically modeled via area sources rather than explicit fault sources. In these cases, planar rupture models—when informed by seismologically constrained nodal planes—provide a more robust alternative.

These findings will be considered when assessing losses and damages within the rapid impact assessment framework of the Global Earthquake Model (GEM). This platform informs several humanitarian communities about the expected impact from destructive events, including the civil protection mechanism of the European Commission and the World Food Programme. Moreover, as a result of this project, we will make any impact estimates available to the EEFIT community for field damage surveys or reconnaissance missions.

8. References

Abrahamson, N. A., Gregor, N., & Addo, K. (2016). BC Hydro ground motion prediction equations for subduction earthquakes. Earthquake Spectra, 32(1), 23–44.

AFAD. (2023). Disaster and Emergency Management Presidency of Ministry of Interior Affairs of Türkiye. 06 February 2023 Pazarcik-Elbistan (Kahramanmaras) Mw: 7.7 – Mw: 7.6 earthquakes report. (in Turkish).

Akkar, S., Sandikkaya, M. A., & Bommer, J. J. (2014). Empirical ground-motion models for point- and extended-source crustal earthquake scenarios in Europe and the Middle East. Bulletin of Earthquake Engineering, 12(1), 359–387.

Alexander, D. (2010). The L'Aquila earthquake of 6 April 2009 and Italian government policy on disaster response. Journal of Natural Resources Policy Research, Vol. 2 No. 4, pp. 325-342.

Asian Disaster Reduction Center (ADRC). (2016). Japan: Earthquake: 2016/04/14 Retrieved from https://www.adrc.asia/view_disaster_en.php?Lang=en&Key=2088

Bindi, D., Massa, M., Luzi, L., Ameri, G., Pacor, F., Puglia, R., & Augliera, P. (2014). Pan-European ground-motion prediction equations for the average horizontal component of PGA, PGV, and 5%-damped PSA at 417 spectral periods up to 3.0 s using the RESORCE dataset. Bulletin of Earthquake Engineering, 12(1), 391-430.

Bommer, J. J., & Akkar, S. (2012). Consistent source-to-site distance metrics in ground-motion prediction equations: A critical review. Journal of Seismology, 16(4), 661–675.

Boore, D. M., Stewart, J. P., Seyhan, E., & Atkinson, G. M. (2014). NGA-west 2 equations for predicting PGA, PGV, and 5%-damped PSA for shallow crustal earthquakes. Earthquake Spectra, 30, 1057–1085.

Casarotti, C., Pavese, A., & Peloso, S. (2009). The seismic response of the San Salvatore hospital of Coppito (L'Aquila) during the earthquake of April 6th, 2009. Progettazione Sismica, 3, 159–172.

Cauzzi, C., Faccioli, E., Vanini, M., & Bianchini, A. (2014). Updated predictive equations for broadband (0.01 to 10 s) horizontal response spectra and peak ground motions, based on a global dataset of digital acceleration records. Bulletin of Earthquake Engineering, 13(6), 1587–1612.

Chiou, B. S. J., & Youngs, R. R. (2014). Update of the Chiou and Youngs NGA model for the average horizontal component of peak ground motion and response spectra. Earthquake Spectra, 30(3), 1117–1153.

Earle, P. S., Wald, D. J., Jaiswal, K. S., Allen, T. I., Hearne, M. G., Marano, K. D., Hotovec, A. J., & Fee, J. M. (2009). Prompt assessment of global earthquakes for response (PAGER)—A system for rapidly determining the impact of earthquakes worldwide: U.S. Geological Survey Open-File Report 2009-1131, 15 p.

EFE. (11 May 2011). "Los dos seísmos se deben a un deslizamiento horizontal de falla de Lorca". ABC. Archived from the original on 11 September 2011. Retrieved 11 May 2011.)

Gallovič, F., Imperatori, W., & Mai, P. M. (2015). Effects of three-dimensional crustal structure and smoothing constraint on earthquake slip inversions: Case study of the Mw6.3 2009 L'Aquila earthquake. Journal of Geophysical Research, 120, 428-449.

Hermanns, L., Fraile, A., Alarcón, E., & Álvarez, R. (2014). Performance of buildings with masonry infill walls during the 2011 Lorca earthquake. Bulletin of Earthquake Engineering, 12(5), 1977–1997.

Huang, J. S., Huang, Y. C., Wang, Y. S., & Lien, Y. N. (2011). Design of a contingency communication network. 13th Asia-Pacific Network Operations and Management Symposium, 21-23 September 2011, Taipei, Taiwan.

Kaklamanos, J., Baise, L. G., & Boore, D. M. (2011). Estimating unknown input parameters when implementing the NGA ground-motion prediction equations in engineering practice. Earthquake Spectra, 27(4), 1219–1235.

Kotha, S. R., Weatherill, G., Bindi, D., & Cotton, F. (2020). A regionally-adaptable ground-motion model for shallow crustal earthquakes in Europe. Bulletin of Earthquake Engineering, 18, 4091-4125.

López-Comino, J. A., Stich, D., Morales, J., & Ferreira, A. (2016). Resolution of rupture directivity in weak events: 1D versus 2D source parameterizations for the 2011, Mw 4.6 and 5.2 Lorca earthquakes, Spain. Journal of Geophysical Research, 121(8), 6608–6626.

Lozano, J. M., Tien, I., Nichols, E., & Frost, J. D. (2024). Impact of ground motion uncertainty evolution from post-earthquake data on building damage assessment. Earthquake Spectra, 40(4), 2430–2455.

Magnitude 5.1 – Spain: Tectonic Summary". United States Geological Survey. 11 May 2011. Archived from the original on 8 June 2011. Retrieved 11 May 2011.

Mai, P.M., & Thingbaijam, K.K.S. (2014). SRCMOD: An online database of finite-fault rupture models. Seismological Research Letters, 85(6), 1348-1357.

Martins, L., & Silva, V. (2021). Development of a fragility and vulnerability model for global seismic risk analyses. Bulletin of Earthquake Engineering, 19, 6719–6745.

Monelli, D., Pagani, M., Weatherill, G., Danciu, L., & Garcia, J. (2014). Modeling distributed seismicity for probabilistic seismic-hazard analysis: Implementation and insights with the OpenQuake engine. Bulletin of the Seismological Society of America, 104(4), 1636–1649.

Montalva, G. A., Bastías, N., & Rodriguez-Marek, A. (2017). Ground-motion prediction equation for the Chilean Subduction Zone. Bulletin of the Seismological Society of America, 107(2), 901–911.

Narlitepe, F., Goksu, C., & Ilki, A. (2024). Comparison of the ratio of spectral response to design accelerations with the observed seismic behavior of RC buildings during February 2023 Türkiye earthquake. 18th World Conference on Earthquake Engineering (WCEE), Milan, Italy.

Pagani, M., Monelli, D., Weatherill, G., et al. (2014). OpenQuake engine: An open hazard (and risk) software for the global earthquake model. Seismological Research Letters, 85(3), 692–702.

Scherbaum, F., Cotton, F., & Smit, P. (2004). On the use of response spectral-reference data for the selection and ranking of ground-motion models for seismic hazard analysis in regions of moderate seismicity: The case of rock motion. Bulletin of the Seismological Society of America, 94(6), 2164–2185.

Silva, V., Crowley, H., Pagani, M., et al. (2014). Development of the OpenQuake engine, the Global Earthquake Model's open-source software for seismic risk assessment. Natural Hazards, 72(3), 1409–1427.

Thompson, E. M., & Worden, C. B. (2018). A ground-motion prediction equation for earthquake-induced landslides. Seismological Research Letters, 89(1), 227–239.

Volpini, A. (2009). L'Ospedale nel sistema dei soccorsi sanitari. Rome: Dipartimento Nazionale della Protezione Civile.

Wald, D. J., Seligson, H., Rozelle, J., Burns, J., & Marano, K. (2020). A domestic earthquake impact alert protocol based on the combined USGS PAGER and FEMA Hazus loss estimation systems. Earthquake Spectra, 36(1), 164–182.

Worden, C. B., & Wald, D. J. (2016). ShakeMap manual: Technical manual, user's guide, and software guide. U.S. Geological Survey.

Yagi, Y., Okuwaki, R., Enescu, B., Kasahara, A., Miyakawa, A., & Otsubo, M. (2016). Rupture process of the 2016 Kumamoto earthquake in relation to the thermal structure around Aso volcano. Earth, Planets and Space, 68(1), 1-6.

Yepes-Estrada, C., Calderon, A., Costa, C., Crowley, H., Dabbeek, J., Hoyos, M., Martins, L., Paul, N., Rao, A., & Silva, V. (2023). Global building exposure model for earthquake risk assessment. Earthquake Spectra, 39(4), 2212-2235.

Zhao, J. X., Zhang, J., Asano, A., Ohno, Y., Oouchi, T., Takahashi, T., Ogawa, H., Irikura, K., Thio, H. K., Somerville, P. G., & Fukushima, Y. (2006). Attenuation relations of strong ground motion in Japan using site classification based on predominant period. Bulletin of the Seismological Society of America, 96(3), 898–913.

Zhao, J. X., Liang, X., Jiang, F., Xing, H., Zhu, R., Hou, Y., Zhang, X., Lan, D. A., Rhoades, K., & Irikura, K. (2016). Ground-motion prediction equations for subduction interface earthquakes in Japan using site class and simple geometric attenuation functions. Bulletin of the Seismological Society of America, 106(4), 1518–1534.